
Combined Endoscopic Optical Coherence Tomography and Laser Induced Fluorescence

50

Jennifer K. Barton, Alexandre R. Tumlinson, and Urs Utzinger

Keywords

Endoscopy • Dual-modality • Fluorescence imaging • Fluorescence spectroscopy • Optical coherence tomography

50.1 Introduction

Optical coherence tomography (OCT) and laser-induced fluorescence (LIF) are promising modalities for tissue characterization in human patients and animal models. OCT detects coherently backscattered light, whereas LIF detects fluorescence emission of endogenous biochemicals, such as reduced nicotinamide adenine dinucleotide (NADH), flavin adenine dinucleotide (FAD), collagen, and fluorescent proteins, or exogenous substances such as cyanine dyes. Given the complementary mechanisms of contrast for OCT and LIF, the combination of the two modalities could potentially provide more sensitive and specific detection of disease than either modality alone. Sample probes for both OCT and LIF can be implemented using small diameter optical fibers, suggesting a particular synergy for endoscopic applications. In this chapter, the mechanisms of contrast and diagnostic capability for both OCT and LIF are briefly examined. Evidence of complementary capability is described. Example published combined OCT–LIF systems are reviewed, one successful commercial instrument is discussed, and example applications are provided.

J.K. Barton (✉) • U. Utzinger
Biomedical Engineering, The University of Arizona, Tucson, AZ, USA

Optical Sciences, The University of Arizona, Tucson, AZ, USA
e-mail: barton@email.arizona.edu

A.R. Tumlinson
Carl Zeiss Meditec, Inc., Dublin, CA, USA

50.2 Background on Optical Coherence Tomography

OCT provides high-resolution, depth-resolved images of scattering tissues. With micron-scale resolution and millimeter depth of imaging, OCT is ideal for examining superficial and optically accessible tissues. Most commonly, the amplitude of the backscattered signal is displayed to yield structural images. In this case, signal originates from index of refraction mismatches. Functional variants described elsewhere of this handbook include polarization-sensitive OCT, which is sensitive to tissue birefringence and optical axis orientation [1–4]; Doppler OCT, which measures the velocity of moving scatterers [5–7]; phase-contrast OCT, which is sensitive to small changes in optical path length [8, 9]; and molecular contrast OCT (MCOCT) [10–12], which includes measurement of changes in the source spectrum due to attenuation by endogenous or exogenous substances [13, 14] as well as detection of processes that yield coherent radiation, e.g., coherent anti-Stokes Raman scattering [15] and second harmonic generation [16, 17]. Several exogenous scattering agents have also been proposed to selectively enhance the OCT signal [18–23]. These additional mechanisms of contrast may augment the diagnostic capability of OCT. MCOCT, similar to LIF, has the potential to identify and quantify the presence of certain endogenous and targeted or untargeted exogenous molecules.

50.2.1 Diagnostic Accuracy of Optical Coherence Tomography

OCT has demonstrated promise for providing accurate diagnoses in a variety of organ sites. Several clinical applications are described in detail in this handbook. Diagnosis and management of retinal disorders, early cancer detection (especially in epithelial tissues), and detection of vulnerable plaque are perhaps the most widely studied applications.

The number of moderate- to large-scale clinical studies performed to assess diagnostic accuracy of OCT is currently modest. Example results from recent *in vivo* human cancer studies and *ex vivo* human artery studies, each using histology as the gold standard, as well as non-histologically confirmed *in vivo* ophthalmic studies, are summarized below. Sensitivity is the percentage of abnormal samples correctly classified, and specificity is the percentage of normal samples correctly classified.

1. *Esophagus*: The performance of endoscopic OCT for the diagnosis and exclusion of dysplasia in patients with Barrett's esophagus was evaluated *in vivo* in 33 patients. Results were the following: sensitivity, 68 %; specificity, 82 %; positive predictive value, 53 %; negative predictive value, 89 %; and diagnostic accuracy, 78 %. Diagnostic accuracy for the four endoscopists ranged from 56 % to 98 %. [24].

In another study of 78 patients with Barrett's esophagus, the ability of OCT to detect high-grade dysplasia and carcinoma, differentiated from benign Barrett's esophagus, low-grade dysplasia, and metaplastic epithelium was evaluated. Sensitivity was 83 % with specificity of 68 %. Positive predictive value was 62 %,

negative predictive value was 87 %, and diagnostic accuracy was 74 %. No cases of invasive adenocarcinoma were missed [25].

2. *Urinary Bladder*: A study utilized the commercial Niris[®] (Imalux) system to examine 52 patients with suspicious lesions based on white-light cystoscopy. While the number of malignant lesions (carcinoma in situ or cancer) was small (14), OCT was able to identify all for 100 % sensitivity. Specificity was fairly low at 65 % [26].

A two-center study examining 80 patients with OCT introduced through the working channel of a rigid cystoscope showed that OCT was able to differentiate benign conditions from urothelial dysplasia, carcinoma in situ, and invasive cancer with 82 % sensitivity and 85 % specificity. Positive predictive value was 51 %, but negative predictive value was 96 %, suggesting that OCT might be used to eliminate some unnecessary biopsies [25]. Further, members of this group performed another study utilizing polarization sensitive OCT. With the additional information available from polarization properties of the epithelium and connective tissue, they were able to increase sensitivity to 94 % and specificity to 84 % for flat malignant bladder lesions, a significantly better result than using conventional OCT [27].

3. *Colon*: Specific image features were found in OCT images of 35 patients with suspected inflammatory bowel disease. Segments affected by ulcerative colitis and Crohn's disease could be differentiated from normal segments with 100 % sensitivity and 78 % specificity [28].

Another study showed that OCT could also differentiate adenoma ($n = 60$) from hyperplastic polyps ($n = 56$) with good sensitivity (92 %) and specificity (84 %) [25].

4. *Cervix*: OCT can be used to identify regions of cervical intraepithelial neoplasia (CIN) and squamous carcinoma in the cervix, although sensitivity and specificity vary depending upon the disease grade used as the threshold between "normal" and "abnormal." In one study of 120 women, utilizing CIN grade 2 as the threshold, a sensitivity and specificity of 85 % and 62 %, respectively, was obtained [29].

In another study, 183 women who were human papillomavirus positive or had abnormal cytology received colposcopy, acetic acid visual inspection, and comprehensive biopsies. The addition of OCT to visual inspection increased sensitivity of detecting lesions greater than cervical intraepithelial neoplasia (CIN) grade 2 from 43 % to 62 %, while decreasing specificity from 96 % to 80 % [30]. A computer algorithm has been developed which can enable high specificity in differentiation of these high-grade lesion. Processing of 152 images in 74 patients yielded a sensitivity of 51 % with 92 % specificity [31].

5. *Skin*: OCT and polarization-sensitive OCT from 104 patients, mainly with basal cell carcinoma, actinic keratosis, and benign lesions, were obtained. While OCT could not reliably diagnose type of lesions, it was able to differentiate normal from lesion areas and identify lesion boundaries. Sensitivity of 79–94 % and specificity of 85–96 % were obtained in differentiating normal skin from lesions [32]. In another study of 112 patients, OCT image features could be

used to distinguish actinic keratosis from normal or sun-damaged skin with 86 % sensitivity and 83 % specificity [33].

6. *Artery*: A study of 323 regions in 8 cadaver hearts compared OCT and intravascular ultrasound (IVUS). The sensitivity/specificity of OCT to fibrous plaque, lipid-rich plaque, and calcified plaque was 91/88 %, 64/88 %, 77/94 %, and 67/97 %, respectively, superior to IVUS results. IVUS sensitivity/specificity was 55/79 %, 63/59 %, 10/96 %, and 76/98 %, respectively, for the same categories [34].

Another study of 128 coronary arterial sites from 17 cadavers, using IVUS and OCT, also demonstrated the superiority of OCT. The sensitivity/specificity of OCT for calcification, fibrosis, and lipid pool was 100 %/100 %, 98 %/94 %, and 95 %/98 %, respectively, which was improved over the best ultrasound modality (integrated backscatter) with sensitivity/specificity of 100 %/99 %, 94 %/84 %, and 84 %/97 %, respectively [35].

7. *Eye*: Despite rarely having gold standard histological verification, OCT is clinically accepted as accurate for the detection and measurement of ocular parameters, such as retinal thickness, presence and width of vitreous adhesion, and presence and width of full thickness macular holes. Therefore, OCT has been used in several Phase III clinical drug trials. OCT has been used to screen for volunteer eligibility (criterion of minimum retinal thickness), to monitor drug effect on retinal thickness [36], and to determine drug-dosing timing based on retinal thickness measurement [37]. In one study of 652 study eyes in a drug trial, grading reproducibility with OCT was found to be high (kappa 0.87–0.91) [38].

While these studies have demonstrated that OCT can provide good to excellent diagnostic accuracy, these authors and others have pointed out limitations. First, most clinically practical (endoscopic) OCT systems have limited resolution. Lacking subcellular resolution, identification of cell types or visualization of markers of neoplasia such as abnormal nuclear size is not directly possible (although statistical image analysis may reveal certain cellular attributes). Even ultrahigh-resolution OCT systems cannot generally visualize subcellular structure at depth in highly scattering human tissue. This restriction can make differentiation between grades of dysplasia/neoplasia difficult with OCT. Given reliance on tissue architecture features for diagnosis, benign conditions such as scarring may be confused as pathology. OCT images also suffer from speckle, which can obscure features and boundaries.

50.3 Background on Laser-Induced Fluorescence

Fluorescence is radiative emission following stimulation of a molecule into an excited state [39]. Fluorescence is characterized by the absorption properties of the molecule, the lifetime of the excited state, the ratio of the radiative versus nonradiative decay rates (quantum yield), and the structure of the vibrational levels of the ground state (emission spectrum). The fluorescence emission spectrum

usually is independent of the excitation wavelength and is red shifted compared to the excitation. The emission spectrum is often a mirror image of the excitation spectrum, separated by the Stokes shift, because the structure of the vibrational levels is similar for the excited and the ground states. Fluorescence spectroscopy contains more information about the molecule's environment than does absorption spectroscopy. For example, upon polarized excitation, small fluorescence molecules exhibit more unpolarized emission compared to large molecules or molecules bound to rigid structures because the fluorescence lifetime limits the reorientation time of the molecule before emission. The fluorescence intensity can be quenched through static and dynamic pathways. Static pathways form new, less-fluorescent molecules through chemical reactions with the quencher and dynamic pathways increase nonradiative decay rates through collisions with the solvent. If two fluorescent molecules are in close proximity and their emission and absorption spectra overlap, energy transfer can occur from the donor molecule to the acceptor (Foerster Resonance Energy Transfer), making the emission characteristics dependent on the distance between the two molecules. The transfer efficiency between the donor and acceptor can also be measured through a decrease of the lifetime of the donor. Fluorescence emission is incoherent thus will not produce speckle.

50.3.1 Fluorophores

Fluorescence in the living tissue originates from endogenous fluorophores but can also be introduced by exogenous contrast agents or generated in genetically modified species expressing fluorescence proteins or enzymes capable of activating chemiluminescence. Endogenous fluorescence can be excited from intracellular constituents such as metabolites and proteins as well as interstitial components such as structural proteins. Several reviewers have discussed the application of endogenous fluorescence and surveyed the biologic fluorophores [40–45]. Endogenous fluorophores in the tissue are available at concentrations in the range of micromolar to hundreds of nanomolar. Their relatively low concentration and preferred excitation at short wavelengths suggest that they may not be amenable to interrogation by MCOCT. In general, endogenous tissue fluorescence with excitation below 300 nm is approximately an order of magnitude stronger than with UV-A (320–400 nm) excitation, and fluorescence emission with blue excitation is approximately another order of magnitude weaker than with UV-A excitation. Proteins are responsible for the high fluorescence efficiency of the tissue excited below 300 nm because many proteins contain the aromatic amino acids such as tyrosine, tryptophan, and phenylalanine [39].

Landmark studies have established a link between cellular metabolism and fluorescence emission [46–48]. Key fluorophores that correlate specifically with cellular activity include the electron carriers NAD and FAD. As a cell changes its metabolic activity, the balance between the reduced (NADH, FADH₂) and oxidized (NAD, FAD) form of the electron carrier shifts correspondingly as the

reduction–oxidation (redox) state of the cell fluctuates. Because only NADH and FAD exhibit significant fluorescence signals, the redox state can be estimated through a ratio of the peak emission values from these molecules assuming their concentrations are inversely linked to the nonfluorescing counterparts.

Type I collagen, one of the main components of the interstitial matrix, exhibits both optical scattering and autofluorescence, two properties that can potentially be exploited as a diagnostic marker of the interstitial matrix using both OCT and LIF. Significant fluorescence has also been noted from elastin fibers and keratin.

Fluorescence emission in the red was observed in animal sarcomas in the beginning of the twentieth century using a Wood's lamp [49] and later confirmed to originate from porphyrins [50]. There may be multiple sources of porphyrins in the tissue, such as incomplete heme-synthesis, microbes, or a by-product of some tumors [51, 52]. Additionally, the authors have shown that a chlorophyll-rich diet increases emission from the colon at 680 nm, which is consistent with the spectral profile of chlorophyll and its metabolites such as pheophorbide-*a* and pyropheophorbide-*a* [52–54], making chlorophyll in diet an important exogenous fluorophore in the colon.

Lipofuscin is ubiquitous as a by-product of frustrated metabolism in the lysosomal compartments of cells throughout the body. Increases in lipofuscin generally indicate a sustained insufficiency of a metabolic pathway and is usually associated with age or disease [55]. A complete lack of lipofuscin where it is usually noted in some degree may indicate a shutdown in metabolism or an extinction of a critical cell type [56].

Current contrast agent developments in molecular imaging can increase the visibility of molecular phenotypes, even though the target of interest might not exhibit itself a strong optical signature. Fluorescence-based reporters can be detected in very low quantities (picomolar, compared to tens of micromolar reporter concentration currently needed for MCOCT). Several exogenous compounds have been approved for in vivo clinical applications, e.g., visualization of the ocular vasculature with fluorescein or indocyanine green (ICG). Those compounds are intravenously injected and made available as systemic fluorescent substrate. Semiconductor nanocrystals compared to conventional fluorophores have relatively narrow and tunable emission spectra and are photochemically stable.

Protoporphyrin IX is an end product of metabolized delta-5-aminolevulinic acid (ALA), and ALA is thought to preferentially accumulate in tumors. Over the last 5 years, several studies have evaluated ALA-induced fluorescence for skin [57, 58], colon [59–61], larynx [62], and bladder cancer detection [63–65]. The measurement of ALA-induced fluorescence is compatible with combined OCT–LIF devices.

50.3.2 Diagnostic Accuracy of Laser Induced Fluorescence

Fluorescence spectroscopy has been proposed for the assessment of patients at increased risk for developing a disease, for demarcation and identification of lesions, and for prognostic follow-up after treatment. Early reports suggested that

quantitative endogenous fluorescence could discriminate between normal and malignant tissues [66]. In the 1980s, Alfano and coworkers reported endogenous fluorescence measurements in vitro [67], and, subsequently, through the advancement in fiber-optic light delivery and detection as well as the development of sensitive and portable spectral analyzers, a multitude of clinical and preclinical endogenous tissue spectroscopy studies have been conducted. Recent review articles summarize the chronological evolution and diagnostic performance of LIF up to the year 2000 [43] and summarize spectroscopic detection of neoplasia [44]. Clinical studies have been performed in the colon, cervix, bronchus, bladder, brain, oral cavity, larynx, skin, bile duct, breast, arteries, and stomach. Here we summarize recent results for several organ sites in Table 50.1. When available, performance of current clinical visual examination is also reported (* in Table 50.1). As with OCT, the diagnostic performance of LIF is highly variable but generally ranges from good to excellent. Recent significant studies in the two most published organ sites are described in additional detail below:

1. *Cervix*: Accurate optical diagnosis of cervical dysplasia could lead to a method where patients with an abnormal cytological screening result are triaged into those who do not need any further intervention and those who need a biopsy or potentially a treatment in the same visit. Several groups have reported recent results including a multicenter clinical trials by MediSpectra [68] with a single wavelength excitation source combined with diffuse reflectance measurements and a point-scanning device as well as SpectRx guided with similar approach [69]. The MediSpectra report indicated a 33 % increase in detection rate for high-grade disease while maintaining the specificity at the level of current clinical practice, while SpectRx also reported reduction in false-positive rate. In 2002 Chang and coworkers [70] as well as Georgakoudi and coworkers [71] published results of their studies on 147 and 44 patients, respectively. Chang reported that more than three to four excitation wavelengths do not improve performance and confirmed previous findings by Ramanujam [72]. He also reported low performance in detecting low-grade disease and distinguishing normal columnar tissue from high-grade disease. Georgakoudi reported results using an analytical model for extracting intrinsic fluorescence [73], reduced scattering and absorption [74], as well as estimates for average number and size of main scatterers [75]. Sensitivity was significantly improved when a combined trimodal approach was used while the specificity was maintained.
2. *Lung*: The LIFE systems from Xillix uses excitation between 380 and 460 nm emission and observes fluorescence in the green and red [76, 77]. The D-Light system[®] from Storz incorporates an additional white-light measurements [78], and the AFI system from Olympus utilizes two additional reflectance channels at 550 and 610 nm [79, 80]. The Pentax bronchoscope SAFE-1000 used blue excitation and observed green autofluorescence [81]. A European multicenter trial with the D-Light system[®] reported increased sensitivity [78] compared with the earlier multicenter trial by Lam et al. [76] with the Xillix system and corrected the sensitivity and specificity of white-light bronchoscopy reported

Table 50.1 Sensitivity and specificity obtained in select LIF clinical studies. Where available, sensitivity and specificity for a standard clinical method is given also in parentheses

Organ site	# Subjects/ samples	Sensitivity	Specificity	Source (year, reference, organization, ex wavelength/notes)
Cervix (colposcopy)	Meta-analysis	Many	Many	2007, [173] MDACC
	1,090	56 %	87 %	2007, [174] Medispectra, 337
	604/1,500	92 % (67 %)	50 % (54 %)	2004, [68] Medispectra, 337, mc, hg
	147/351	71 %	77 %	2002, [70] UT, multi ex, hg
	44/84	92 %	71 %	2002, [71] MIT, trim, SIL-Bx, nonSIL
	95/381	79 % (79 %)	78 % (76 %)	1996, [175] UT, 337, 380, 460, hg
Ovary	49/249	88 %	93 %	2012, [87] UA, 270–550
	30	100 %	69 %	2012, [176] UA, 365, imaging
	4	N.A.	N.A.	2011, [112] Groningen, Folate-FITC, intrao
	22/97	100 %	91 %	2009, [177] Manipal, 325
Fallopian tube	47	73 %	83 %	2011, [88] BCCA, imaging
Lung (w/ bronchoscopy)	62	91 % (51 %)	26 % (50 %)	2006, [81] Hong Kong, 380–460
	1,173/1,978	82.3 % (57.9 %)	58.4 % (62 %)	2005, [78] Storz, mc, hg
	32/62	80 %	83 %	2004, [80] Olympus
	173/864	67 % (25 %)	66 % (90 %)	1998, [77] Xillix, mc, hg
Oral cavity (w/ examination)	120	N.A.	N.A.	2009/10, [178, 179] Houston, 405, vis
	44/50	98 %	100 %	2009, [180] BCCA, 400–460, hg, vis
	4/4 (images)	91 % (75 %)	86 % (43 %)	2005, [181, 182] UT, visual
	15/91	96 %	96 %	2003, [98] MIT, trim
	76/343	100 % (100 %)	88 % (83 %)	2002, [183] UT, multi ex
	56/179	100 %	51 %	2002, [184] Munich, ALA,375–440
	50/137	88 %	57 %	AF
	7/199 (72)/(214)	100 % (99 %)	51 % (43 %)	ALA&AF (WL)
	15/45	94 % (76.5 %)	100 % (100 %)	1998, [185] UT,MDACC, 337, 365, 410
	Breast	6	N.A.	N.A.
N.A.		N.A.	N.A.	2009, [186] Manipal, 325
17/104		100 %	96 %	2008, [187] MIT, multi ex
3		N.A.	N.A.	2007, [99] Storz, Ductoscopy
18/47		54 %	91 %	2005, [188] UW, multi ex
32/56		70 %	92 %	2003, [101, 116] UW, multi ex
63/911		99 %	99 %	1997, [189], Indore, 337

(continued)

Table 50.1 (continued)

Organ site	# Subjects/ samples	Sensitivity	Specificity	Source (year, reference, organization, ex wavelength/notes)
Colon (w/ colonoscopy)	21	N.A.	N.A.	2013, [96] UA, 270–440
	88	Better than WL	N.A.	2012, [92] Asahikawa, AFI
	75	92 % (68 %)	N.A.	2001/10, [90, 190] PINPOINT, 400–450
	64	84 % (90 %)	60 % (64 %)	2007/8, [89, 191] AFI, 395–475
	NA/177	80 %	92 %	1992, [192] Wellman, 337
Barrett's esophagus	22	100 %	Increase	2012, [102], Amsterdam, AFI, NBI, HRE
	37/148	74 %	85 %	2003, [103] Wellman, 400
	16	100 %	97 %	2001, [104], MIT, 337, 397, 412, trim
	53/141	76 %	63 %	2003, [193] Lausanne, 505
Bladder	14/56	N.A.	N.A.	2013, [109] 308
	21	N.A.	N.A.	2012, [108], 650
	25/52	100 %	100 %	2003, [106] Singapore, 280, 330
	25/43	95/84 %	42/88 %	2001, [107] Munich, AFI alone, ALA & AFI
	75/130	95 %	73 %	1998, [105] Wellman, 337
Brain	3/13	N.A.	N.A.	2010, [110] UC Davis, 337 lifetime
	26/120	100 %	76 %	2001, [194] VU, primary tumor
		97 %	95 %	2004, [195] data from [194]

by Lam. The AFI system was tested on a small sample size, and only abnormal-appearing sites were included in the analysis [80]. A relatively high false-positive rate was reported which limits the positive predictive value [82], and difficulties in distinguishing preinvasive lesions and benign conditions were mentioned. However, a trial with the Pentax system also reported increased sensitivity but reduced specificity [81].

3. *Skin*: A skin autofluorescence reader has been developed to assess advanced glycation end products (AGEs) which show a fair correlation with collagen cross-link and AGE content of the skin (AGE Reader I, DiagnOptics BV Groningen, Netherlands) [83]. Such reading could be a predictor of health outcomes in diabetic patients [84] or could determine cardiovascular risk [85, 86].
4. *Ovary*: Tissue fluorescence was found to be statistically different in normal ovarian tissue between women at high risk for developing ovarian cancer versus women at normal risk especially in postmenopausal women; this result can potentially guide oophorectomy [87]. With the recent hypothesis that ovarian cancer might originate in the fallopian tube, it has been demonstrated that autofluorescence can be measured in the fallopian tubes in situ [88].
5. *Colon*: Xillix and Olympus developed autofluorescence (AF) colonoscopes that illuminate tissue in the violet–blue range. Several randomized trials comparing

AF endoscopy in the colon to standard video endoscopy, narrowband imaging (NBI), or high-resolution endoscopy have been published very recently. The outcomes of these studies have been mixed, with some indicating these AF endoscopes reduce polyp miss rate [89–92], especially for inexperienced coloscopists, and others showing no significant improvement of AF over other technologies [93–95]. Most recently UV imaging has been proposed to improve the detection rate of polyps [96, 97].

6. *Oral Cavity*: Two companies have created a visual autofluorescence system for the examination of the oral cavity. The VelScope™ (LED Medical) and Identafi™ (Remicalm) illuminate the tissue with specific excitation pattern, while the clinician observes the tissue fluorescence through filtered spectacles. The VelScope™ uses blue (400–460 nm) excitation light, while the Identafi™ uses light at 405 nm in combination with green reflectance. The devices have been identified as ideal for oral cancer screening but also for tumor margin delineation. Clinical performance is supported by previous studies using single point spectroscopy and multiple excitation wavelengths [98].
7. *Breast*: While there were limited reports of clinical translation of LIF for breast cancer imaging, there exists a commercial implementation of 1.3 mm diameter ductoscope with autofluorescence imaging capabilities using the DAFE system (Richard Wolf GmbH) [99]. Previously research with fiber-optic probes reported that diffuse reflectance spectroscopy did not improve sensitivity and specificity of fluorescence spectroscopy [100, 101].
8. *Esophagus*: Esophageal cancer detection was investigated with technologies similar to the one used for colonoscopy [102], and autofluorescence imaging combined with high-resolution endoscopy was found to have ideal sensitivity. In addition when combined with narrowband reflectance imaging, a reduced false-positive rate was demonstrated. Earlier work showed that single point spectroscopy at 400 nm excitation was most useful for clinical application [103], while others demonstrated excellent diagnostic performance using fluorescence at 337, 397, and 412 nm excitation [104].
9. *Bladder*: Initial results on bladder cancer diagnosis with autofluorescence [105, 106] as well as ALA-induced fluorescence were promising [107], and recently imaging systems have been developed to acquire NIR autofluorescence [108] or allow pulsed UV laser delivery [109].
10. *Brain*: Tumor demarcation was investigated in the brain using endoscopic fluorescence lifetime measurements [110] and also fluorescence and reflectance spectroscopy [111].
11. *Exogenous Contrast Agents*: Significant advances in intraoperative optical imaging of exogenous contrast agents have been reported recently. For example, folate-targeted fluorescein isothiocyanate (FITC) fluorescence was used to guide tumor debulking in ovarian cancer patients [112]; patency of bypass grafts were studied in patients using intravascular ICG [113]; and sentinel lymph node mapping was demonstrated in the esophagus in animals [114] and also applied in human studies for breast cancer lymph node mapping using open architecture equipment [115]. General lymphatic imaging was

demonstrated using ICG [116]. Aminolevulinic acid (ALA)-induced protoporphyrin IX fluorescence has been studied in several animal models. Its application was studied for peritoneal micrometastasis of ovarian cancer in a rodent animal model and showed that detection rate significantly increased, and fluorescence intensity in tumor versus surrounding tissue increases by 1.5 [117]. Such an approach could be combined with endoscopic devices such as the D-Light system[®] (Karl Storz, Germany); however, human clinical studies have not yet been reported.

50.4 Advantages of a Dual Modality System

The complementary nature of information provided by OCT and LIF (coherent backscatter versus incoherent fluorescence emission) creates the possibility that the combination of OCT and LIF may be more sensitive to tissue function and pathology than either modality alone. The two types of information may also facilitate signal interpretation and increase specificity. Viewing this potential advantage from two different perspectives, cross-sectional OCT images may help to correct and interpret LIF spectra, or LIF imaging/spectra may help to guide and interpret OCT images.

From the first perspective, LIF spectra may be difficult to interpret because they may be influenced by unknown subsurface structures. Spectra obtained at different lateral locations on an apparently smooth, homogeneous surface can vary in intensity and spectral shape. Without depth-resolved anatomical information, it may be difficult to determine if the variation is due to changes in tissue function, type, or thickness. For example, in a layered epithelial/stromal tissue, a relative decrease in the intensity of the fluorescence signal associated with collagen could be due to a true lessening of the fluorescence emission of the stroma or could be caused by a thickening of the overlying epithelium. Another example is given in Fig. 50.1. An OCT image/LIF spectra pair is shown, obtained from the luminal surface of an approximately 3 mm diameter bronchus of excised sheep lung. The spectral shape of the LIF signal is relatively constant, but the intensity is highly nonuniform. The OCT image shows clearly that strong LIF signal corresponds to locations with subsurface cartilage, indicating that the LIF intensity variation is due to normal anatomy.

Quantitative measures of tissue anatomy obtained with OCT can be used to correct LIF data. Several attempts have been made to separate tissue optical properties, such as scattering, absorption, and intrinsic fluorescence from extrinsic fluorescence, and to calibrate fluorescence measurements for illumination and detection conditions. The collected fluorescence depends on optical transport within the tissue [82, 118] and geometrical sensor sample relations [119–121]. LIF intensity is highly dependent upon the probe–sample separation, and OCT can provide this geometrical information with high accuracy. In fact, if only point LIF measurements are being obtained, only A-scan OCT capability is needed. A correction algorithm has been described by Warren et al. [119] using ultrasound A-mode data. A model of the fluorescence intensity was developed and verified with both Monte Carlo

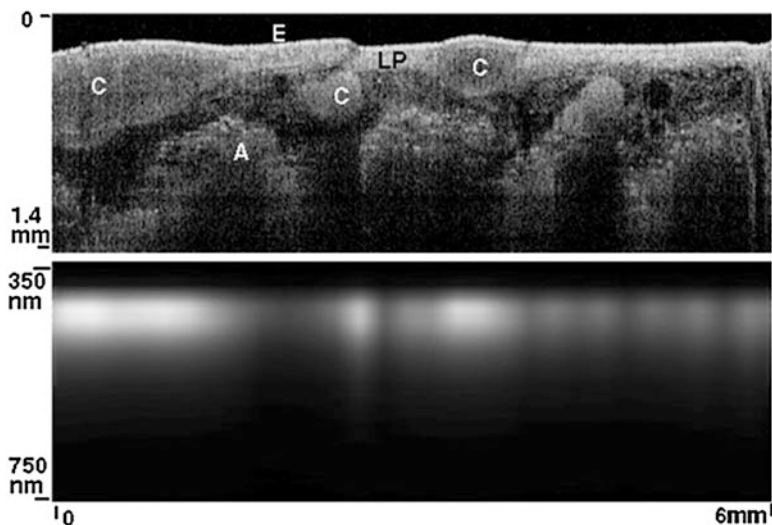


Fig. 50.1 OCT image (*top*) and LIF spectra (*bottom*) of excised sheep lung bronchus. Note the increase in emission intensity at lateral locations corresponding to subsurface cartilage (*C*). Other abbreviations: epithelium (*E*), lamina propria (*LP*), alveoli (*A*)

simulations and empirical data. A correction equation goes as $S_c = S_m/R^n$, where S_m is the measured fluorescence intensity, R is the probe–tissue separation, and $n = 1.1$ for aorta and 2 for theoretical, isotropic fluorescence emission.

Using mathematical models, the particular photon traveling paths can be predicted with a priori knowledge of the illumination and collection geometry, a diffuse reflection measurement, and assumptions about scattering and absorption properties. Zhang and coworkers developed a method that allows extraction of intrinsic fluorescence in semi-infinite media based on fluorescence and diffuse reflectance measurements under the same geometrical configuration [122], which subsequently has been used in several clinical studies as an analytical model. Sung et al. developed a similar analytical approach for two-layered tissue to predict intrinsic fluorescence from the stroma and epithelium separately [123]. This model depends on the epithelial thickness, a number that can be easily obtained with OCT. Fluorophore concentration can also be more accurately determined using tissue scattering and fluorophore depth measurements obtained from OCT. Yuan et al. corrected the measured concentration of a known fluorophore (Cy5.5 dye) in a phantom (tube of dye submerged in intralipid) [124]. This method could be employed to help quantify accumulation of, e.g., an exogenous dye in a discrete tumor. It would be less useful for correcting measurements of distributed endogenous fluorophores, although it could be modified to estimate true contributions from a buried layer (e.g., collagenous stroma) if optical properties and fluorophore concentration of tissue layers are assumed to be homogeneous.

From the second perspective, LIF imaging can guide OCT measurements and clarify inconclusive OCT scans. OCT provides a microscopic view, and thus in

many applications complete screening of the area of interest is impractical, necessitating a guidance technique. LIF imaging, which commonly has high sensitivity but low specificity, can be an ideal method to identify regions of interest for OCT imaging. A simple method of LIF-guided OCT can be implemented by using an OCT daughter probe in the surgical channel of a large endoscope. Additionally, LIF has the potential to clarify OCT scans containing little information due to homogeneous tissue with features below the resolution limit of OCT, such as might be found in a cellular tumor or scar tissue.

Several studies have shown the value of combining OCT and LIF. Kuranov et al. [125] used OCT and LIF to image neoplasms in the cervix and found that these two modalities combined produced fewer false-positive results than either modality alone: abnormally increased fluorescence due to inflammatory reactions was clearly differentiated from cancer by OCT; conversely, OCT-detected atypical structure could be clarified with LIF to simply be a mature scar. Another study [25] found that the PPV of fluorescence cystoscopy of flat bladder lesions was only 16 %, which could be increased to 43 % in addition of OCT. The data suggest that 78 % of biopsies based on fluorescent-positive findings could be avoided, if areas were classified as normal when OCT imaging revealed a regular layered structure.

50.5 Instrumentation Design Considerations

Combined OCT–LIF systems can be essentially two separate systems simply physically packaged together at the tissue location or can share optical and mechanical parts, light sources, and/or digital processing components. There are many possible variations; here we list some of the design considerations and some current/possible implementations. Design considerations for system combination include the type of OCT and LIF systems desired (e.g., full field or scanning OCT, point or imaging LIF), the spectral range of the light source(s) and LIF emission, the choice of endoscope materials, and safety. General optical design considerations are also discussed.

50.5.1 OCT and LIF Systems

Because various types of OCT systems are discussed in detail elsewhere in this handbook, they will not be discussed here. In general, LIF capability can be added to any type of OCT system, although the sharing of components is facilitated if the scan types are common (e.g., both one, two, or three dimensional scanning and full field). An appropriate method of signal separation (spectral, temporal, or spatial) is required.

Steady-state LIF measurements require a light source with a well-defined output spectrum, a conduit to transport the excitation light to the sample, illumination and collection optics, and a conduit to transport the emitted light back to a spectral analyzer for optical detection. Instrumentation for fluorescence measurements is well described by Lakowicz [39], and here we focus on spectral compatibility and common in vivo measurement limitations.

One of the major challenges in fluorescence detection is the signal to background ratio. Background signals are caused by instrument autofluorescence (see Sect. 50.5.4), ccc from the light source, and scattering within the spectral analyzer. Because endogenous signals can be weak, background signals need to be avoided. Out-of-band illumination suppression should reach 10^{-5} or 10^{-6} for endogenous tissue fluorophore measurements, especially in excitation ranges where the fluorescence efficiency is low (blue to green). Because the amount of collected instrument background is also dependent on the sample reflectivity, traditional subtraction of the sample signal by the instrument response to a negative standard (e.g., a measurement in water) has its limitations. As a rule of thumb, instrument background should be kept below 10–30 % of the sample signal. Traditionally, illumination and collection paths have been constructed separately [126] to reduce system autofluorescence. Irradiance levels on excitation optics are significantly higher than on collection optics making it necessary to incorporate autofluorescence reduction techniques in the illumination conduit and optical elements at the endoscope tip. In typical applications, the collection conduit will receive a significant amount of excitation light backscattered by the sample. If the stray light suppression capabilities of the detection system are exceeded (a spectrograph might have 10^{-4} suppression), the backscattered excitation light can also contribute to the signal background. This can be avoided by dampening excitation light in the detection path with long-pass filters before the emitted light is spectrally analyzed.

50.5.2 Spectral Range of LIF Sources and OCT Sources

For LIF, short-arc lamps have been used as a standard low-cost excitation source when coupled to an excitation monochromator or dielectric band-pass filters. Example radiance data for mercury–xenon and xenon lamps are shown in Fig. 50.2, top panel. Their broad emission range allows wavelength tunability, but a common disadvantage of short-arc lamps is the limited ability to focus light into small optical fibers. A large variety of laser modules has been developed for confocal microscopy, and most of these lasers are compact and sufficiently transportable for endoscopic fluorescence measurements. Example sources are shown in Fig. 50.2 and abbreviated as XeCl, xenon chloride (308 nm emission); HeCd, helium–cadmium (325 nm); N₂, nitrogen (337 nm); Ar, argon (351, 364, 458, 488, and 514 nm); YAG, neodymium YAG (1,064, 532 nm); and HeNe, helium–neon (543, 633 nm). Because of the small Stoke's shift of most fluorophores, narrowband sources are preferred to enable efficient collection efficiency of emission light and rejection of excitation light. In contrast, OCT sources are by necessity broadband, with spectral widths of tens to hundreds of nanometers. Also, OCT sources are generally centered in the NIR, to enable greatest depth of imaging in highly scattering tissue. The light source emission spectra for some OCT sources (short-pulsed lasers, swept-wavelength lasers, and superluminescent diodes) are shown in Fig. 50.2. Also shown in Fig. 50.2 is the extinction spectrum of three tuned nanoshells (exogenous scattering agents) [127].

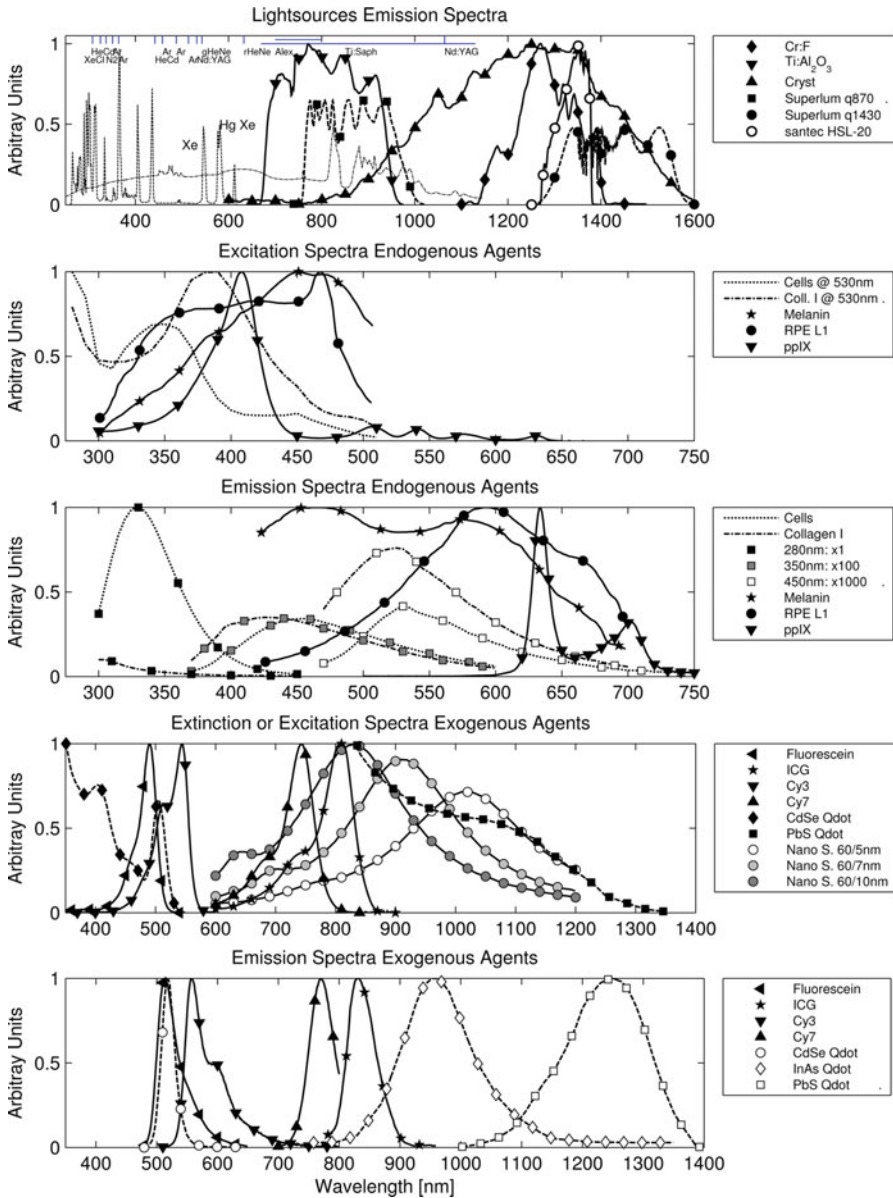


Fig. 50.2 Common light sources, absorbers, and emitters for combined OCT and LIF: *First panel*, illustration of common fluorescence excitation and OCT light sources. Xenon (*Xe*) and mercury–xenon (*Hg–Xe*) short-arc lamps are illustrated (Courtesy of Photon Technology International, Inc.). Published data from OCT sources using titanium sapphire (Ti:Al₂O₃) laser [196], chromium:forsterite (Cr:F) [197] and photonic crystal fibers (Cryst) [198], commercial superluminescent diodes (Superlum Broadlighters q870 and q1430), as well as spectrum of commercial swept source (santec, HSL-20) are shown. Excitation spectra of endogenous

50.5.3 Excitation and Emission and Range of Fluorophores

Epithelial tissues usually exhibit a strong fluorescence peak at 280 nm excitation and 350 nm emission, which is associated with tryptophan fluorescence (Fig. 50.2, bottom panel, cell emission at 280 nm excitation). Cells excited at UV-A wavelengths show strong fluorescence from NADH, which has a maximum at 350 nm excitation and 450 nm emission (Fig. 50.2, cell emission at 350 nm excitation), whereas the oxidized form NAD is not fluorescent [39]. Conversely, FAD fluoresces at a maximum at 450 nm excitation (blue) and 535 nm emission (Fig. 50.2, cell emission at 450 nm excitation), whereas the reduced form FADH₂ fluoresces minimally. Lipofuscin has a very broad excitation and emission spectra. The excitation spectrum is notable in particular because its peak at 470 nm is comfortably above the strong excitation bands of many other materials. Fluorescence from interstitial matrix is dominated by collagen; average fluorescence emission from polymerized collagen that was reconstituted from rat tail type I fragments is shown in Fig. 50.2 middle and bottom panel. Typical emission at 280 nm excitation/300 nm emission (consistent with tyrosine), 320 nm excitation/400 nm emission (consistent with the enzymatic cross-links lysyl hydroxypyridoxyl and hydroxylysyl hydroxypyridoxyl), and 370 nm excitation/450 nm emission (consistent with the nonenzymatic cross-links vespersyl and crossline) can be observed. Unfortunately, at many excitation wavelengths, these collagen emission spectra overlap with the emission observed from cell suspensions. Porphyrins show an excitation maximum at 410 nm and two emission maxima at 630 and 690 nm, while the peak at 630 nm is substantially more intense (Fig. 50.2, protoporphyrin IX). Emission spectra from exogenous fluorophores fluorescein; cyanine dyes Cy3, Cy7, and ICG; and CdSe/InAs quantum dots are also shown in Fig. 50.2. Some of these agents have NIR excitation and/or emission.

Figure 50.2 illustrates that endogenous fluorescence, targeted fluorescence imaging, and optical coherence tomography can be spectrally incorporated because most endogenous components do not absorb or emit within the OCT illumination spectral range, and some exogenous agents are available outside that range. If spectral overlap occurs, LIF and OCT need to be time or spatially multiplexed. Spectral overlap has been used to advantage in one application [128], with simultaneous



Fig. 50.2 (continued) components are illustrated in the *second panel*: reconstituted collagen type I gel and epithelial cell suspension (OVCA 430) data is shown at 530 nm emission [199, 200]. Protoporphyrin IX [201] and melanin and lipofuscin granules extracted from RPE cells are illustrated [55]. Emission spectra corresponding to the compounds from the second panel are illustrated in the *third panel*: emission of collagen type I gel and an epithelial cell suspension is shown at 280, 350, and 450 nm excitation. The *fourth and fifth panels* illustrate excitation and emission spectra of exogenous agents: the absorption and emission of fluorescein (Molecular Probes/Invitrogen, ph9) is compared to a CdSe semiconductor nanocrystal [202, 203]. ICG, a clinically used NIR absorber, is illustrated [204]. Cyanine dyes are illustrated with examples of indocarbocyanine (Cy3) and indotricarbocyanine (Cy7) [201]. Extinction of gold nanoshells on a 60 nm silica core is illustrated as a potential OCT scattering contrast agent [127]. Selected quantum dot emission spectra from CdSe [202, 203], InAs [202], as well as PbS [205] are shown

OCT/ICG imaging in the eye's fundus. In this case, the same superluminescent diode (793 nm center wavelength, 22 nm spectral full width at half maximum) was used for OCT imaging and for excitation of ICG. The key in this implementation was proper selection of the dichroic filter separating backscattered source light (directed to the OCT detector) from fluorescence emission (directed to the LIF detector). This selection minimized distortion of the source correlation function and maximized collection efficiency of fluorescence emission. Excellent simultaneous OCT and ICG images were obtained. However, use of the same source for OCT and fluorescence excitation could become increasingly difficult as either the source bandwidth increases or fluorophore emission intensity decreases, unless very large Stoke's shift NIR-excitable agents become available.

A strategy to provide greater spectral separation has been described [129]. This custom system included a mode-locked Ti:sapphire laser and a 0.9 numerical aperture water immersion objective to generate simultaneous en face optical coherence and two-photon-excited fluorescence images. An image of a green fluorescent protein expressing drosophila embryo was presented; presumably endogenous fluorophore distribution could be imaged as well. Because fluorescence occurred at a much shorter wavelength range, no difficulties were encountered separating the fluorescence from the backscattered light. However, implementation of this method in an endoscopic fashion would be technically challenging because of high peak-power needs, three-dimensional scanning requirements, and the need to control probe-tissue separation.

50.5.4 Materials

As described above, many interesting endogenous fluorophores are best excited at ultraviolet wavelengths that also cause autofluorescence in most optical materials. Many glasses and polymers exhibit autofluorescence that is similar in spectral shape and range to the fluorescence of endogenous tissue fluorophores [130]. Because probe autofluorescence can easily become significant compared to the tissue signal, each component of the OCT-LIF system should be considered for autofluorescence, particularly if the excitation wavelength lies in the UV. The location of the element within the system is equally important as the absorption and emission characteristics of the material. Autofluorescence from an optically thick piece of fiber is generally more significant than from the same material used in a thin window. Additionally, isotropically emitted fluorescence is more easily collected from an element located near focus than from a lens or window located far from focus or in a low-numerical-aperture portion of the beam path. Lenses and windows made of fused silica and CaF_2 have low fluorescence under UV-A excitation and good NIR transmission and are recommended throughout the beam path. Thick windows near the tissue should be restricted to lowest fluorescence glasses, although very thin windows of other glasses and even some low-fluorescence plastic films may be acceptable [131]. Usually, some fluorescent materials must be used despite the best attempts to avoid them. For example,

the emission from even “low-fluorescence” ultraviolet transmitting optical epoxies is significant, and care should be taken to keep glue joints thin [132]. The jacketing materials available on many commercially available communications grade fibers ideal for OCT fluoresce strongly. Although fiber choice could be restricted only to low-fluorescence jacketed materials, it is often more practical to simply shield the fiber from UV-A excitation. This approach of hiding the fluorescent material behind absorbent material, a dichroic filter, or simply out of the beam path is the most flexible and commonly used. Care should be taken with items outside the device that may also autofluoresce, including tissue index matching gels, preservation media, culture plates, or wax mounting blocks.

50.5.5 Safety

The tip of a combined OCT–LIF endoscope is either in contact with or at a close distance to a tissue surface or body fluid and therefore should be analyzed for potential hazards. A thorough analysis of potential risks and protection against those risks are a requirement for human subject studies. Hazards include electrical shock hazards, clinical hazards, material toxicity hazards, and radiation hazards. Of unique importance to combined OCT–LIF systems is the fact that both systems may be operated concurrently, requiring cumulative radiation exposure analyses. Radiation exposure in the UV poses a different hazard than in the visible/NIR. UV exposure is a cumulative hazard due to the potentially ionizing energy of each photon (exposure limits can be calculated for repeated exposure over days), whereas visible and NIR light exposure is analyzed for potential thermal injuries. “Blue-light hazard” is unique to eye exposure, caused by free radical release due to interaction with visual photopigments [133]. Threshold limit values for radiation exposure are defined by several standardization organizations: The American National Standards Institute (ANSI) publishes maximal permissible exposure levels [134]; the American Conference of Governmental Industrial Hygienists (ACGIH) publishes similar threshold limit values (TLV) and biological exposure indices [135]. Applications which intentionally introduce light into the eye should verify that standards set for ophthalmic instruments ISO 15004-2 are met in addition to laser safety standards. In contrast to the above-listed standardization organizations, the International Commission on Non-Ionizing Radiation Protection (Oberschleissheim, Germany) makes their guidelines available online at no cost and publishes them in *Health Physics*. Usually the threshold limit values are expressed for laser beam [136, 137] and incoherent exposure [138, 139] of the eye and skin. For broadband UV exposure (<400 nm), the biologically effective radiation (device emission weighted by the biologic action spectrum, which is normalized at 270 nm) should not exceed the TLV for melano-compromised skin and eye (3 mJ/cm^2) [138]. The TLV for the skin and eye has also been recommended for the cervix in a guidance document developed by the US Food and Drug Administration’s Center for Device and Radiological Health (CDRH) [140]. For the wavelength range of 0.38–1.4 μm , exposure limits are governed by

thermal injury to the skin and eye. Unfortunately, the authors are not aware of any studies evaluating combinational effects of NIR radiation and UV exposure.

50.5.6 Optical Design Considerations

The optical design of a combined system is a result of an attempt to optimally control the photon paths in the tissue for each modality, while meeting material constraints in the optical path and separating the signals (chromatically, spatially, or temporally) to the appropriate detector. The useful signal in OCT depends on photons that undergo a single scattering event in a nearly backscattering direction. The confocal design of typical OCT systems helps reject photons that take any other path. Lateral resolution is dependent upon the beam cross section at a given depth. Usually, a balance between lateral resolution and depth of focus is struck in order to avoid axially scanning the objective [141]. Conversely, LIF photons are typically allowed to take a circuitous path: the excitation light may be scattered multiple times before it is absorbed. If fluorescence conversion occurs, the emission spectrum of the intrinsic fluorescence will be modified as the emitted photons wander randomly through the tissue until they are absorbed by chromophores or released at the tissue surface. The path taken, and volume subsequently probed by the LIF system, depends on the tissue absorption and scattering properties as well as factors determined by the probe geometry: the insertion angles of excitation photons, the distance along the surface the collection to point (source-detector separation distance – SDS), and the angles over which the photons are collected. Fiber-optic probes have been proposed for preferential depth-sensitive fluorescence sensing with the use of variable illumination and collection apertures [142, 143], illumination collection distances [143–146], and illumination collection angles [147–149].

Monte Carlo analysis of specific fiber-optic probe implementations on media with tissue-like optical properties and their associated experimental verifications show trends that are useful in designing an LIF probe. First, it is critical to control the distance between the illumination/collection fibers and the tissue for quantitative tissue analysis [145, 150]. When the illumination and collection areas are superimposed at the tissue surface ($SDS = 0$), either by means of single illumination–collection fiber in contact with the tissue, or a spacer distal to a group of fibers that allows the illumination–collection areas to diverge over the same tissue area, the probe will be primarily sensitive to superficial layers less than 400 μm deep [142, 144, 145]. Similarly shallow tissue sampling can be achieved when source and collection fibers are separated at the tissue surface but are inclined towards each other to cause an overlap of the fiber numerical apertures in the superficial tissue [148, 149, 151]. The average probed depth can be increased from 700 to 1,200 μm by placing normally incident illumination and collection fibers that are directly in contact with the tissue at increased separation [142, 144, 145]. Evidence with diffuse reflectance modeling suggests that the probed depth can be increased yet further by inclining the fibers away from each other [152]. In general, greater overlap of the numerical apertures of the illumination and collection fibers improves collection efficiency while the

expected probing depth decreases. The lateral extent of a collected LIF photon's path has been relatively unexplored, although lateral resolution somewhat larger than the SDSs could be expected. Increasing the fiber core diameter and numerical aperture increases the light gathering capacity of the collection fiber but may have effects on the depth of collected fluorescence that depends upon the configuration. In cases with fibers in contact with the tissue, the size of the illumination and collection area introduces a superposition of many SDSs, while the numerical aperture of the fiber introduces a superposition of many angles of insertion and collection. In addition to the depth selectivity provided by SDS, some geometries appear to be optimally sensitive to fluorophore distribution rather than scattering properties of the tissue [153, 154]. Knowledge of tissue layer thicknesses from OCT images could help in the selection of optimal LIF illumination/detection fiber configurations.

In the case where the majority of information from LIF derives from direct emission from a fluorophore in a relatively superficial tissue layer, a confocal arrangement delivers significant advantages. Confocal arrangements are common in fluorescent microscopes because they have the potential to deliver high-resolution imaging with high contrast. High resolution derives from the tightly limited photon paths allowed by the confocal arrangement. Contrast is enhanced by spatial filtering of out-of-plane, unwanted fluorescence, including that from the optics of the instrument itself. In combination with point-scanning OCT, the two confocal modalities will share similar design needs and constraints.

Because OCT systems generally utilize single-mode fibers and LIF systems utilize multimode fiber (to optimize the collected fluorescence emission signal), the most straightforward OCT–LIF endoscope design utilizes separate fibers for each modality. Maintaining separate conduits for OCT and LIF minimizes the cross talk between the systems and helps maintain high signal-to-background ratio. The proximal coupling optics between the fibers and sources/detectors are also simplified. However, other fiber configurations are possible. Dual-clad fibers consist of a central core with two layers of cladding. The core can be made single mode, whereas the inner cladding has a large radius and high-numerical aperture (multimode). OCT light is channeled to the sample through the core. LIF excitation light can be carried by the core (if compatible) or the inner cladding. Remitted OCT, excitation, and emission light are coupled into the core and inner cladding. In addition to coupling light into the dual-clad fiber, the proximal optics must spatially separate returned OCT light which has propagated through the core from that which has taken unwanted paths through the inner cladding, and spectrally separate the OCT and fluorescence emission. Dual-clad fibers have successfully been used in OCT–LIF systems [155–158], and one system is described in more detail below.

Under certain conditions, multimode fiber bundles can also be used to carry both OCT and LIF signals, with the benefit of eliminating distal scanning. The use of a Fourier-domain OCT system incorporating a common-path interferometer mitigates the effect of wavefront distortions through the multimode fiber bundle, although cross talk between fibers can be an issue. A system was recently demonstrated that utilized a common fiber bundle and CCD detector for both OCT and fluorescence confocal imaging [159].

50.6 Combined OCT–LIF System Examples

Of many potential implementations, three designs are discussed below: a free-space ophthalmic, an endoscopic OCT–LIF point-scanning, and an OCT–LIF surface-imaging system. The free-space system is conceptually more simple, appropriate for ophthalmic imaging, and introduces several system design elements. Combined OCT–LIF endoscopes allow examination of a variety of mucosal tissues *in situ*. Clinically it is interesting to have tools that can monitor the disease noninvasively or to guide traditional biopsy techniques. Because tissue degrades structurally and biochemically with time after excision, *in vivo* endoscopic studies potentially have the most accurate and conclusive diagnostic capability. At the same time, the small packages and biocompatibility requirements of endoscopes present a challenge to the designer. The two very different combined OCT–LIF endoscopes presented here embody the design principles discussed in the previous section.

50.6.1 Scanning Laser Ophthalmoscope with OCT and Fluorescence

Fluorescence angiography with fundus photography or confocal scanning laser ophthalmoscopy (SLO) is an established technique to evaluate the circulation of the retina. Recently, fundus autofluorescence (FAF) imaging, primarily observing lipofuscin concentration, has been shown to be a valuable marker in multiple disease states [160]. Optical coherence tomography has revolutionized clinical retinal practice due to its ability to obtain high-resolution cross-sectional images in this highly stratified tissue that clearly differentiate disease states. The development of combined OCT–LIF systems for retinal imaging is a logical progression for streamlining the retina research and practice. Commercial devices (SPECTRALIS[®], Heidelberg Engineering) [161] for comprehensive evaluation of retinal disorders provide similar functionality to a previously described combined research system [128, 162]. A system diagram of the research system from the Podoleanu group is illustrated in Fig. 50.3. This instrument is a good example of the use of a confocal architecture for both OCT and LIF, where confocality in the OCT channel is achieved by use of a single-mode fiber (small core size behaves as a pinhole) and the confocality of the SLO and indocyanine green (ICG) fluorescence channels reject out-of-focus light. The scanning confocal architecture of the SLO is highly compatible with time-domain, en face OCT. In this system, uniquely, a single light source is used for both OCT and fluorescence excitation, as the excitation spectrum of ICG (peak near 800 nm, see Fig. 50.2) overlaps with clinically useful OCT imaging wavelengths. Dichroic filters separate reflected light from fluorescence emission. Depth-resolved OCT can be collected simultaneously with en face SLO and ICG fluorescence. The resulting images from all modalities can be presented separately or superimposed. SPECTRALIS[®] OCT differs architecturally from the described research system by providing greater independence between the two systems. The system combines an independent, spectral-domain OCT system to an SLO system at a dichroic splitter. The two modalities are individually optimized for beam scanning speed, spectral band,

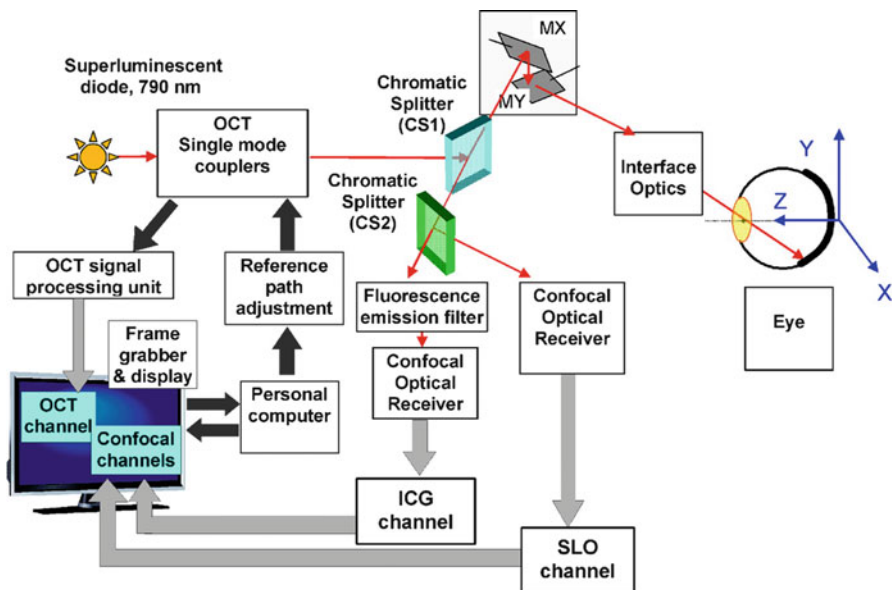


Fig. 50.3 System diagram of a free-space ophthalmic OCT/SLO/ICG imaging system. MX, MY: galvanometer mirrors of the x–y scanning pair (Reprinted from Ref. [162])

and beam geometry. The SLO provides a fast, registered fundus view, which the system uses as an aiming aid for the OCT beam, and maintains the ability to co-register SLO-based en face images and OCT B-scans.

50.6.2 Dual-Clad Fiber OCT–LIF Endoscope

An all-fiber OCT and point-scanning fluorescence endoscope was developed in the laboratory of Li [163]. The system, illustrated in Fig. 50.4, combines an OCT swept-source laser near 1,300 nm with blue laser light (488 nm) into the core of a dual-clad fiber. Reflected OCT and blue laser light, as well as fluorescence emission remitted from the tissue, are coupled into both the core and inner cladding of the dual-clad fiber. A custom dual-clad fiber coupler returns the core light back to the OCT subsystem. Weak fluorescence emission and strong reflected blue laser light are not detected by the OCT subsystem as they do not interfere with the OCT source and are outside the spectral bandwidth of the OCT optics and detector. The same fiber coupler directs light from the inner cladding to a multimode fiber. OCT and blue excitation light are eliminated with a band-pass filter prior to detection of fluorescence emission light by a photomultiplier tube. In the endoscope, optics consisted of a glass spacer and GRIN lens, which focus the light. A distal micromotor-mounted 45° reflector directs the light out the side of the endoscope and enables circumferential scanning. In an initial study, this endoscope was able to image *ex vivo* rabbit esophagus with approximately 14 μm OCT resolution to the

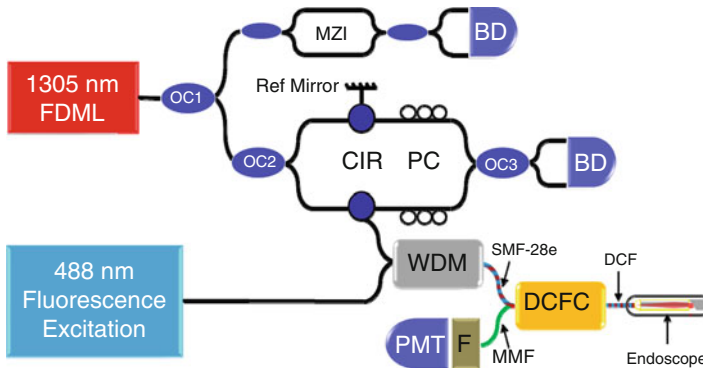


Fig. 50.4 Diagram of a combined OCT/point-scanning fluorescence system utilizing dual-clad fiber in the endoscope. *FDML* Fourier-domain mode-locking fiber laser, *OC* optical coupler, *MZI* Mach-Zehnder interferometer, *CIR* circulator, *PC* polarization controller, *BD* balanced detector, *WDM* wavelength division multiplexer, *DCFC* dual-clad fiber coupler, *PMT* photomultiplier tube, *F* band-pass filter; *green*, multimode fiber (*MMF*); *blue/red*, dual-clad fiber (*DCF*); *black*, single-mode fiber (*SMF-28e*) (Reprinted from Ref. [163])

depth of the muscularis mucosa. The fluorescence channel detected injected fluorescein sodium and possibly identified blood vessels.

50.6.3 Endoscopic OCT/Surface Fluorescence Imaging

Separate fiber conduits are used to carry OCT and LIF signals in the third example of a dual modality device [164]. A system and distal optics diagram is given in Fig. 50.5. In this instrument, spectral-domain OCT and surface-magnifying chromoendoscopy (SMC) are combined. SMC utilizes high magnification surface imaging with the FDA-approved vital dye methylene blue to visualize crypt patterns in the colon. Either the absorption or, as in this case, the fluorescence of methylene blue can be detected. The proximal subsystem construction was simplified by utilizing separate fibers. The OCT subsystem is a conventional spectral-domain system. The SMC subsystem consists of a red laser diode coupled via a microscope objective into a 30,000 element fiber bundle. To detect the fluorescence emission image, the fiber bundle face is imaged onto a low-noise CCD camera, through dichroic and emission filters. At the distal end of the endoscope, the fiber bundle is centered on a spacer/GRIN lens combination. Four OCT fibers (only one used) are arranged concentrically. A right-angle prism directs light out the side of the endoscope. An annulus limits the numerical aperture of the detected fluorescence emission light to prevent total internal reflection in the GRIN lens. Judicious use of aberrations including chromatic dispersion and astigmatism enables the SMC channel to focus to an image plane adjacent to the outer cylindrical surface of the covering glass envelope, while OCT light is focused to a diffraction-limited spot 190 μm inside the tissue. Linear movement of the optics within the glass envelope provides overlapping

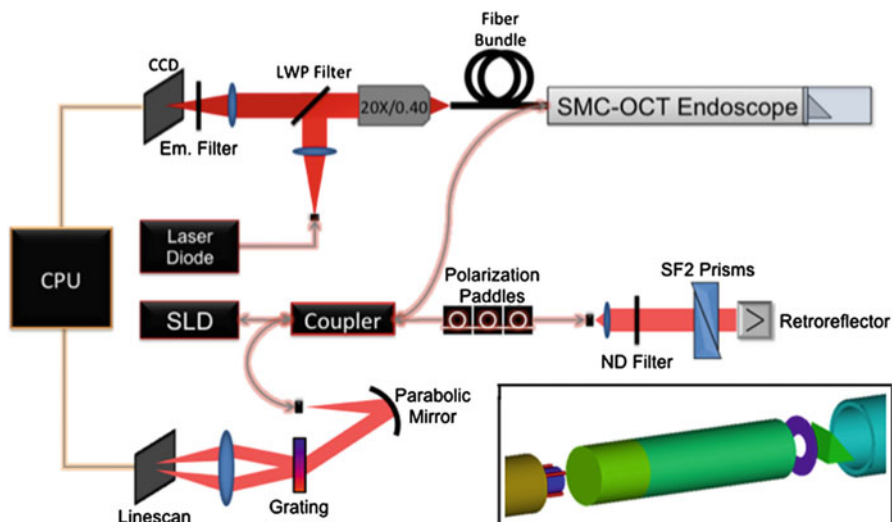


Fig. 50.5 Diagram of an endoscopic OCT/surface fluorescence imaging system. Fluorescence and OCT sources are fiber coupled into endoscope. A long-wave pass (*LWP*) filter is used to reflect excitation light and pass emission light in the SMC proximal setup, while neutral density (*ND*) filters attenuate OCT source power. Charge-coupled devices (*CCD*) are used to detect signal in each modality, and data is electronically transmitted to the central processing unit (*CPU*). Inset shows the distal tip optics. From left to right: *gold*, positioning ferrule; *navy*, 30,000 element fiber bundles; *red*, OCT single-mode fibers; *green*, spacer; *teal*, GRIN lens; *purple*, annulus; *green*, right-angle prism; *blue*, protective class envelope (Adapted from Ref. [164])

circular en face SMC images and a single cross-sectional OCT image. This system has been used to obtain time-serial images of cancer development in the mouse colon.

50.7 Example Applications

To conclude this chapter, we describe three example applications of combined OCT–LIF system: imaging of the human eye with an in-air OCT/autofluorescence system, ex vivo imaging of rat ovary with an endoscopic OCT/autofluorescence spectroscopy system, and in vivo imaging of mouse colon with an endoscopic OCT/surface fluorescence imaging system. Each of these examples provides evidence that the two modes of data obtained are complimentary.

50.7.1 Human Eye with Macular Degeneration

Automatic superposition of the multimodality images enable correlations to be made between en face autofluorescence measurements and cross-sectionally

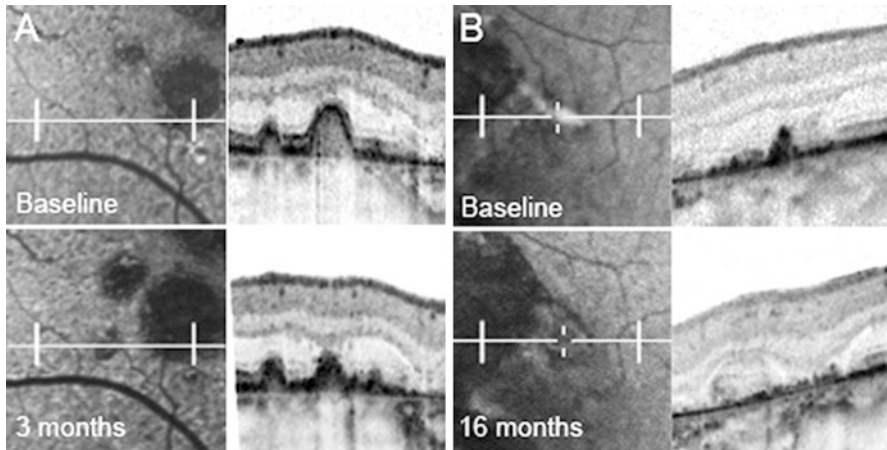


Fig. 50.6 Simultaneous autofluorescence and OCT imaging in the eyes with developing geographic atrophy (GA) due to age-related macular degeneration. (a) At baseline, a dome-shaped elevation OCT correlates with drusen material. There is irregular but still preserved fluorescence (*upper left*). After 3 months, a small lesion with decreased FAF has developed, and continuing structural changes are seen in OCT (*lower left*). (b) At baseline, there is an accumulation of hyperreflective material in the OCT scan that is spatially collocated with an intensely increased FAF signal (*upper right*). After 16 months, the hyperreflective material has disappeared, and retina structure is distorted on OCT (*lower right*) (Reprinted from Ref. [166])

visible structural changes in the retina. Autofluorescence signal arises primarily from lipofuscin concentration, normally located in the retinal pigment epithelium (RPE) [165]. OCT contrast originates primarily from the segregation of cellular structures in the neural retina, with cell bodies yielding low reflectance while their complex neural processes tend to scatter more light. The RPE contains a high concentration of melanin, which is strongly absorbed by OCT wavelengths. When the RPE is disrupted, the signal from the underlying choroidal tissue is hyperintense. For example, Fig. 50.6 shows two cases in which changes in both OCT and autofluorescence track the temporal progression of geographic atrophy in the perilesional zone, where macular degeneration-related vision loss is most likely to progress [166]. In the first case (A), structural thickening (drusen material) with normal fluorescence precedes an apparently decreasing thickness of drusen material but an abnormal development of decreased fluorescence. In a second case (B), an area of localized hyperreflectance in OCT is correlated with a region of hyperintense autofluorescence in a region that eventually shows structural changes in OCT that point clearly towards cell layer loss and development of geographic atrophy. Utilizing these two modalities in a combined instrument may be useful to track and predict retinal disease progression, elucidate mechanisms of disease, and evaluate the effects of therapeutic agents with greater accuracy and resolution.

50.7.2 Rat Ovary

A combined OCT–LIF was used to acquire images and spectra of 54 excised rat ovaries [167]. This system combines a time-domain OCT system with an autofluorescence point-spectroscopy system. Due to the integration time needed for autofluorescence spectroscopy, the relatively slow speed of a time-domain system was not the time-limiting factor. The endoscope combined a GRIN lens-based imaging system for the single-mode OCT fiber, with separate unlensed multimode excitation and emission collection fibers [168]. While this study was *ex vivo*, the endoscope was used in preparation for future minimally invasive *in vivo* studies. The goal of this study was to determine if OCT and/or LIF could distinguish between ovaries from normal cycling animals, postmenopausal ovaries (follicle depletion induced by *i.p.* injection of 4-vinylcyclohexene diepoxide or VCD), and ovaries with atypia or neoplasms induced by 7, 12-dimethylbenz-alpha-anthracene (DMBA). VCD was administered for 20 days at a dose of 160 mg/kg *i.p.* Three to five months later, some animals had a DMBA soaked suture (approximately 110 μg DMBA) placed through the right ovary. One to five months after suture insertion, the animals were sacrificed and the ovaries excised. Excess fat and connective tissue were trimmed prior to imaging; no superficial blood contamination was apparent.

Figure 50.7 shows a sequence of OCT images/LIF spectra and histology from a normal cycling ovary, VCD-treated follicle-deplete ovary, a VCD-/DMBA-treated ovary with atypia (follicular remnant degeneration), and a VCD-/DMBA-treated ovary with neoplastic cysts. In the cycling ovary, antral follicles and the bursa are seen. The VCD-treated ovary is much reduced in size, and only dense stroma with surface fat is seen, as would be expected in a follicle-deplete, postmenopausal ovary. Follicular remnant degeneration in the DMBA-treated ovary manifests as a multitude of small hypointense regions, whereas the cancerous cysts are large hypointense regions. The OCT images show excellent correspondence to histology at the tissue architecture level. While the DMBA-treated ovaries clearly appeared abnormal, a determination of neoplasia could not be made since the markers of cancer (e.g., abnormally large or irregular nuclei) were not identifiable at the resolution of this OCT system. Therefore, it appears that OCT may be of use in identifying abnormal-appearing ovaries but by itself cannot make a determination of atypical changes or neoplasia. Molecularly targeted contrast agents (absorption or scattering) could be of use to increase OCT's sensitivity and specificity to cancer.

With 325 nm excitation wavelength, the LIF spectra show peaks at approximately 390 and 450 nm and absorption at 420 nm, associated with collagen fluorescence, NADH fluorescence, and hemoglobin absorption, respectively. In the normal cycling ovary, the magnitude of the 450 nm peak is greater than the 390 nm peak, and the dip at 420 nm is well defined. This suggests that a relatively large amount of NADH and hemoglobin is present in the ovary. In contrast, LIF spectra from the follicle-deplete ovary is dominated by the 390 nm peak, indicative

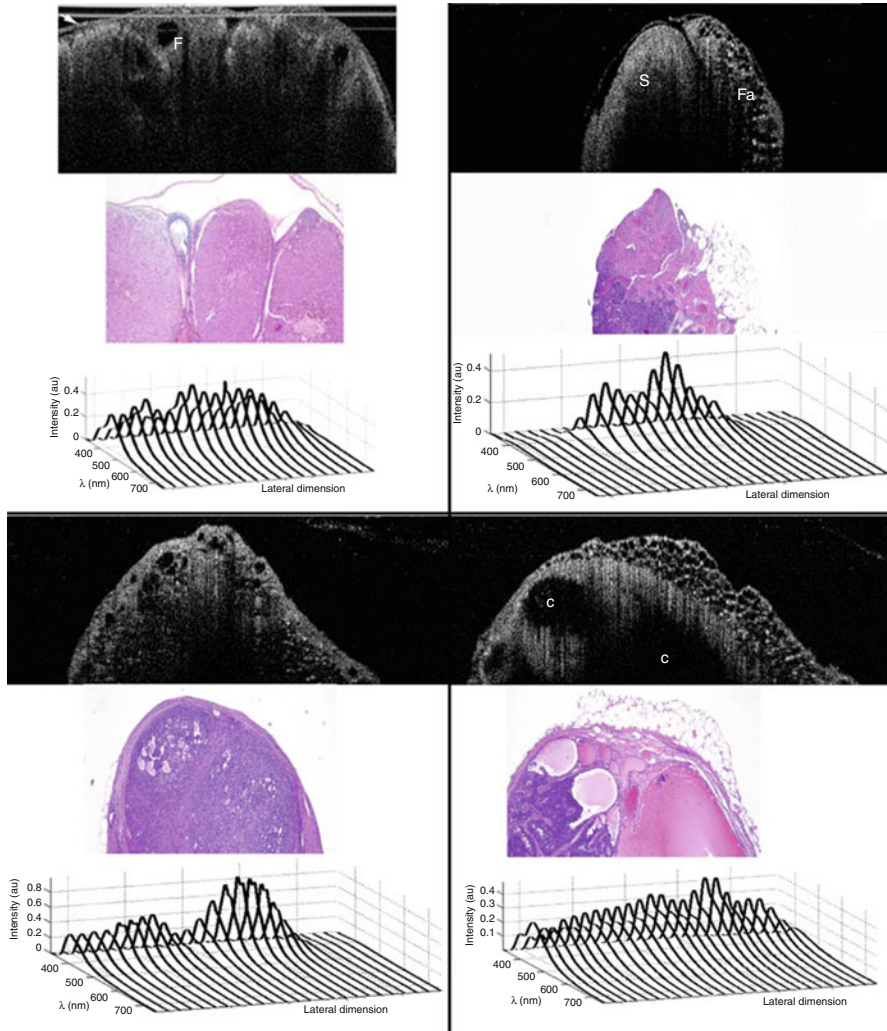


Fig. 50.7 A sequence of OCT images, LIF spectra, and histology from a normal cycling ovary (*top left*), VCD-treated follicle-deplete ovary (*top right*), a VCD-/DMBA-treated ovary with atypia-follicular remnant degeneration (*bottom left*), and a VCD-/DMBA-treated ovary with neoplastic cysts (*bottom right*). The normal cycling ovary shows follicular cysts (*F*), whereas the follicle-deplete ovary has only dense stroma (*S*) and fat (*Fa*). Many small abnormal cysts are seen in the atypical ovary, and large abnormal cysts (*C*) are seen in the neoplastic ovary. OCT images correlate well with histology. LIF shows a trend towards increased 450:390 nm fluorescence emission ratio in metabolically active ovaries (either normal cycling or atypical/neoplastic) compared to the follicle-deplete ovary. OCT images are 5 mm lateral \times 1.4 mm deep, except normal cycling which is 4 mm lateral. Histology is to same scale as OCT. LIF data are presented over the same lateral range as the OCT images (Adapted from Ref. [167])

of high relative collagen content and less metabolic activity. There is also a relatively small amount of vasculature as seen from the LIF spectra (less pronounced dip at 420 nm), which was confirmed histologically. The DMBA-treated ovaries both show a relatively high 450 nm fluorescence peak and pronounced 420 nm absorption, similar to the cycling ovary. A comparison between groups shows statistically significant differences in the ratio of 390:450 nm fluorescence intensity of the cycling and cancerous groups, as compared to follicle-deplete group. A follow-on study investigating 162 freshly excised ovaries also saw changes in OCT structure and fluorescence emission spectra of normal versus cancerous ovaries [169].

In summary, the feasibility of using the combined OCT–LIF system to determine the presence of atypical and neoplastic changes in the ovary was shown. Different structures such as cysts, fatty regions, and follicular remnant degeneration were easily identified in the OCT images. There was preliminary evidence from this study that atypical cellular changes might be located in the regions identified by irregularly sized hypointense regions in the OCT images, but OCT could not directly distinguish atypical cells and areas of cancer. The LIF spectra provided information about hemoglobin content as well as the metabolic activity of the ovary and displayed significant changes between follicle-deplete emission ratios and both cycling and neoplastic emission ratios. Therefore, this study suggested that by utilizing combined OCT and LIF data, it may be possible to distinguish between cycling, follicle-depleted, non-atypical, atypical, and neoplastic ovaries.

50.7.3 Mouse Colon

The OCT–LIF endoscope provides access to the distal 3 cm of the mouse colon. In vivo monitoring in a mouse model may enable extrapolation about the capability of OCT–LIF to identify cancer in a human patient as well as aid in the development of chemotherapeutics. The normal mouse colon is approximately 300 μm thick with an average crypt measuring 100 by 20 μm . Epithelial cancers start as aberrant crypt foci (ACF) that are little larger than a collection of several crypts and may become large adenomas over 1 mm in diameter. In the digestive tract, chromophores common to other tissues (including collagen, NADH, and hemoglobin) are present in combination with those found in the digested food.

Several in vivo studies have been performed in mouse colon with dual modality OCT–LIF instruments. In some studies [170, 171], OCT images have been used to identify areas of the mouse colon that are abnormal and to use this data to isolate matching autofluorescence spectra associated with tumors. Statistically significant differences between normal and tumor tissues have been observed in LIF spectra, but the variation in fluorescence signal in normal tissue limits sensitivity and specificity. Details in the OCT image such as changes in mucosal layer thickness, or presence of adventitia surrounding the colon can be associated with fluctuations in the autofluorescence spectra. This highlights the complementary,

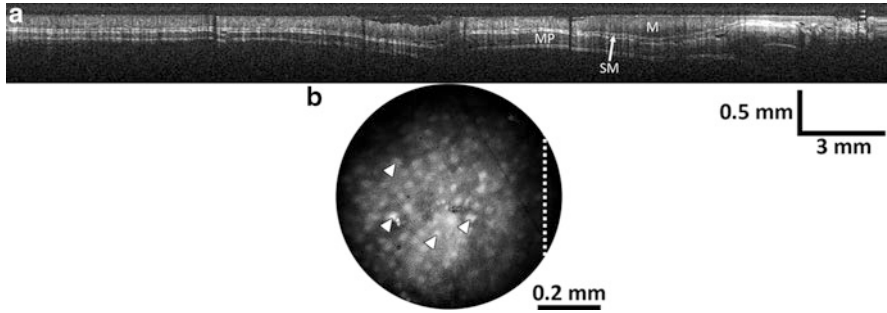


Fig. 50.8 Optical coherence tomography (OCT) image scanning the full 30 mm of the in vivo mouse colon (a) and surface magnifying chromoendoscopy (SMC) image taken at one location in the mouse colon (b). The layered structures of the colon, including the mucosa (M), submucosa (SM), and muscularis propria (MP), are easily identified in the OCT image, while arrows in the SMC image point to individual colonic crypts, and the white dotted line corresponds to the scan line of the specific OCT image (Reprinted from Ref. [164])

but nonorthogonal, nature of the datasets and the potential to improve fluorescence diagnostics with knowledge of the underlying tissue structure.

Rather than detecting autofluorescence, targeted fluorescent contrast agents can be used. In one study [172], the colon was lavaged with Cy5.5 dye conjugated to a vascular endothelial growth factor (VEGF) fragment, and a 633 nm HeNe laser was used for LIF excitation. The dye preferentially attached to VEGF receptor-2. Results showed significantly higher, but also highly variable, fluorescence emission intensity over adenoma. Also, a large variation in fluorescence emission was seen in regions of the colon which appeared normal on OCT images. A correlation was seen between fluorescence emission intensity of images of frozen sections and images of sections immunostained for VEGF receptor-2. These results suggest that expression of VEGF receptor-2 is not homogeneous in disease and that the LIF information provides information on molecular events not visible with OCT. Time-serial imaging might be performed to determine if adenoma with high levels of VEGF receptor-2 expression have more aggressive growth patterns.

An example image pair of mouse colon taken with the endoscopic OCT/surface fluorescence imaging system described above is given in Fig. 50.8. The top image shows a cross-sectional OCT image of the full 30 mm length of the mouse colon. The bottom image shows a 700 μm diameter field of view fluorescence surface-magnifying chromoendoscopy image at one location. In this case, the surface image with contrast agent enables high-contrast image of the crypt structure of the mouse colon. Due to the small size and low contrast of the crypts, this information cannot be seen in the OCT image. A targeted dye could be used to not only help visualize the structure of aberrant crypt foci (putative earliest stage of disease) but also overexpression of cell surface markers associated with early disease.

50.8 Conclusion

In this chapter, existing combined OCT–LIF endoscopic systems were described, and potential improvements in resolution and collection efficiency with alternative optical designs were presented. There is evidence that the combination of OCT and LIF is synergistic in several respects. First OCT can provide information about subsurface structures that can aid interpretation of LIF spectra. Second, quantitative measures of tissue layer thickness and probe–tissue separation can be used in models that seek to extract intrinsic fluorescence or correct for tissue distance. Third, LIF can provide information on tissue characteristics which are not visible to OCT. Finally, if criteria are properly developed for both modalities, the combination of the two may increase sensitivity and/or specificity to disease. Future work will help define the applications most enhanced by this dual modality approach.

References

1. G. Yao, L.V. Wang, Two-dimensional depth-resolved Mueller matrix characterization of biological tissue by optical coherence tomography. *Opt. Lett.* **24**(8), 537–539 (1999)
2. C.K. Hitzenberger, E. Gotzinger, M. Sticker, M. Pircher, A.F. Fercher, Measurement and imaging of birefringence and optic axis orientation by phase resolved polarization sensitive optical coherence tomography. *Opt. Express* **9**(13), 780–790 (2001)
3. J.F. de Boer, T.E. Milner, Review of polarization sensitive optical coherence tomography and Stokes vector determination. *J. Biomed. Opt.* **7**(3), 359–371 (2002)
4. J. Zang, S. Guo, W. Jung, J.S. Nelson, Z. Chen, Determination of birefringence and absolute optic axis orientation using polarization-sensitive optical coherence tomography with PM fibers. *Opt. Express* **11**(24), 3262–3270 (2003)
5. J.A. Izatt, M.D. Kulkarni, S. Yazdanfar, J.K. Barton, A.J. Welch, In vivo bidirectional color Doppler flow imaging of picoliter blood volumes using optical coherence tomography. *Opt. Lett.* **22**(18), 1439–1441 (1997)
6. V.X.D. Yang, M.L. Gordon, B. Qi, J. Pekar, S. Lo, E. Seng-Yue, A. Mok, B.C. Wilson, I.A. Vitkin, High speed, wide velocity dynamic range Doppler optical coherence tomography (Part I): system design, signal processing, and performance. *Opt. Express* **11**(7), 794–809 (2003)
7. G. Liu, W. Jia, V. Sun, B. Choi, Z. Chen, High-resolution imaging of microvasculature in human skin in-vivo with optical coherence tomography. *Opt. Express* **20**(7), 7694–7705 (2012)
8. M. Sticker, C.K. Hitzenberger, R. Leitgeb, A.F. Fercher, Quantitative differential phase measurement and imaging in transparent and turbid media by optical coherence tomography. *Opt. Lett.* **26**(8), 518–520 (2001)
9. C. Joo, T. Akkin, B. Cense, B.H. Park, J.F. de-Boer, Spectral-domain optical coherence phase microscopy for quantitative phase-contrast imaging. *Opt. Lett.* **30**(16), 2131–2133 (2005)
10. C. Yang, Molecular contrast optical coherence tomography: a review. *Photochem. Photobiol.* **81**(2), 215–237 (2005)
11. S.A. Boppart, A.L. Oldenburg, C. Xu, D.L. Marks, Optical probes and techniques for molecular contrast enhancement in coherence imaging. *J. Biomed. Opt.* **10**(4), 41208 (2005)
12. B.E. Applegate, C. Yang, J.A. Izatt, Theoretical comparison of the sensitivity of molecular contrast optical coherence tomography techniques. *Opt. Express* **13**(20), 8146–8163 (2005)
13. U. Morgner, W. Drexler, F.X. Kartner, X.D. Li, C. Pitris, E.P. Ippen, J.G. Fujimoto, Spectroscopic optical coherence tomography. *Opt. Lett.* **25**(2), 111–113 (2003)

14. K.D. Rao, M.A. Choma, S. Yazdanfar, A.M. Rollins, J.A. Izatt, Molecular contrast in optical coherence tomography by use of a pump-probe technique. *Opt. Lett.* **28**(5), 340–342 (2003)
15. W.A. Benalcazar, S.A. Boppart, Nonlinear interferometric vibrational imaging for fast label-free visualization of molecular domains in skin. *Anal. Bioanal. Chem.* **400**, 2817–2825 (2011)
16. Y. Jiang, I. Tomov, Y. Wang, Z. Chen, Second-harmonic optical coherence tomography. *Opt. Lett.* **29**(10), 1090–1092 (2004)
17. M.V. Sarunic, B.E. Applegate, J.A. Izatt, Spectral domain second-harmonic optical coherence tomography. *Opt. Lett.* **30**(18), 2391–2393 (2005)
18. C. Loo, A. Lin, M. Lee, J.K. Barton, N. Halas, J. West, R. Drezek, Nanoshell-enabled photonics-based imaging and therapy of cancer. *Technol. Cancer Res. Treat.* **3**, 33–40 (2004)
19. A.M. Winkler, P.F. Rice, R.A. Drezek, J.K. Barton, Quantitative tool for rapid disease mapping using optical coherence tomography images of azoxymethane treated mouse colon. *J. Biomed. Opt.* **15**(04), 041512 (2010)
20. M. Kirillin, M. Shirmanova, M. Sirotkina, M. Bugrova, B. Khlebtsov, E. Zagaynova, Contrasting properties of gold nanoshells and titanium dioxide nanoparticles for optical coherence tomography imaging of skin: Monte Carlo simulations and in vivo study. *J. Biomed. Opt.* **14**(2), 021017 (2009)
21. H. Cang, T. Sun, Z.Y. Li, J. Chen, B.J. Wiley, Y. Xia, X. Li, Gold nanocages as contrast agents for spectroscopic optical coherence tomography. *Opt. Lett.* **30**, 3048–3050 (2005)
22. T.M. Lee, A.L. Oldenburg, S. Sitafalwalla, D.L. Marks, W. Luo, F.J. Toublan, K.S. Suslick, S.A. Boppart, Engineered microsphere contrast agents for optical coherence tomography. *Opt. Lett.* **28**, 1546–1548 (2003)
23. Y. Changhuei, L.E.L. McGuckin, J.D. Simon, M.A. Choma, B.E. Applegate, J.A. Izatt, Spectral triangulation molecular contrast optical coherence tomography with indocyanine green as the contrast agent. *Opt. Lett.* **29**(17), 2016–2018 (2004)
24. G. Isenburg, M.V. Sivak, A. Chak, R.C. Wong, J.E. Willis, B. Wolf, D.Y. Rowland, A. Das, A. Rollins, Accuracy of endoscopic optical coherence tomography in the detection of dysplasia in Barrett's esophagus: a prospective, double-blinded study. *Gastrointest. Endosc.* **62**(6), 825–831 (2005)
25. E. Zagaynova, N. Gladkova, N. Shakhova, G. Gelikonov, V. Gelikonov, Endoscopic OCT with forward-looking probe: clinical studies in urology and gastroenterology. *J. Biophotonics* **1**(2), 114–128 (2008)
26. A. Karl, H. Stepp, E. Willmann, A. Buchner, Y. Hocaoglu, C. Stief, S. Tritschler, Optical coherence tomography for bladder cancer – ready as a surrogate for optical biopsy? Results of a prospective mono-centre study. *Eur. J. Med. Res.* **15**(3), 131–134 (2010)
27. N. Gladkova, O. Streltsova, E. Zagaynova, E. Kiseleva, V. Gelikonov, G. Gelikonov, M. Karabut, K. Yunusova, O. Evdokimova, Cross-polarization optical coherence tomography for early bladder-cancer detection: statistical study. *J. Biophotonics* **4**(7–8), 519–532 (2011)
28. P. Consolo, G. Strangio, C. Luigiano, G. Giacobbe, S. Pallio, L. Familiari, Optical coherence tomography in inflammatory bowel disease: prospective evaluation of 35 patients. *Dis. Colon Rectum* **51**(9), 1374–1380 (2008)
29. J.K. Gallwas, L. Turk, H. Stepp, S. Mueller, R. Ochsenukhn, K. Friese, C. Dannecker, Optical coherence tomography for the diagnosis of cervical intraepithelial neoplasia. *Lasers Surg. Med.* **43**(3), 206–212 (2011)
30. N. Wulan, N. Rasool, S.E. Belinson, C. Wang, X. Rong, W. Zhang, Y. Zhu, B. Yang, N.J. Tresser, M. Mohr, R. Wu, J.L. Belinson, Study of the diagnostic efficacy of real-time optical coherence tomography as an adjunct to unaided visual inspection with acetic acid for the diagnosis of preinvasive and invasive neoplasia of the uterine cervix. *Int. J. Gynecol. Cancer* **20**(3), 422–427 (2010)
31. W. Kang, X. Qi, N.J. Tresser, M. Kareta, J.L. Belinson, A.M. Rollins, Diagnostic efficacy of computer extracted image features in optical coherence tomography of the precancerous cervix. *Med. Phys.* **38**(1), 107–113 (2011)

32. M. Mogensen, T.M. Joergensen, B.M. Nürnberg, H.A. Morsy, J.B. Thomsen, L. Thrane, G.B. Jemec, Assessment of optical coherence tomography imaging in the diagnosis of non-melanoma skin cancer and benign lesions versus normal skin: observer-blinded evaluation by dermatologists and pathologists. *Dermatol. Surg.* **35**(6), 965–972 (2009)
33. V. Korde, G. Bonnema, W. Xu, C. Krishnamurthy, J. Ranger-Moore, K. Saboda, L. Slayton, S. Salasche, J. Warneke, D. Alberts, J.K. Barton, Using optical coherence tomography to evaluate skin sun damage and precancer. *Lasers Surg. Med.* **39**, 687–695 (2007)
34. J. Rieber, O. Meissner, G. Babaryka, S. Reim, M. Oswald, A. Koenig, T.M. Schiele, M. Shapiro, K. Theisen, M.F. Reiser, V. Klauss, U. Hoffmann, Diagnostic accuracy of optical coherence tomography and intravascular ultrasound for the detection and characterization of atherosclerotic plaque composition in ex-vivo coronary specimens: a comparison with histology. *Coron. Artery Dis.* **17**(5), 425–430 (2006)
35. M. Kawasaki, B.E. Bouma, J. Bressner, S.L. Houser, S.K. Nadkarni, B.D. MacNeill, I.K. Jang, H. Fujiwara, G.J. Tearney, Diagnostic accuracy of optical coherence tomography and integrated backscatter intravascular ultrasound images for tissue characterization of human coronary plaques. *J. Am. Coll. Cardiol.* **48**(1), 81–88 (2006)
36. Diabetic Retinopathy Clinical Research Network, A randomized trial comparing intravitreal triamcinolone acetonide and focal/grid photocoagulation for diabetic macular edema. *Ophthalmology* **115**(9), 1447–1449 (2008)
37. F.G. Holz, W. Amoaku, J. Donate, R.H. Guymer, U. Kellner, R.O. Schlingemann, A. Weichselberger, G. Staurengi, SUSTAIN Study Group, Safety and efficacy of a flexible dosing regimen of ranibizumab in neovascular age-related macular degeneration: the SUSTAIN study. *Ophthalmology* **118**(4), 663–671 (2011)
38. F.C. DeCroos, C.A. Toth, F.A. Folgar, S. Pakola, S.S. Stinnett, C.S. Heydary, R. Burns, G.J. Jaffe, Characterization of vitreoretinal interface disorders using OCT in the interventional phase 3 trials of ocriplasmin. *Invest. Ophthalmol. Vis. Sci.* **53**(10), 6504–6511 (2012)
39. J.R. Lakowicz, *Principles of Fluorescence Spectroscopy* (Kluwer Academic/Plenum, New York, 1999)
40. G.A. Wagnieres, W.M. Star, B.C. Wilson, In vivo fluorescence spectroscopy and imaging for oncological applications. *Photochem. Photobiol.* **68**, 603–632 (1998)
41. M.A. Mycek, B.W. Pogue, *Handbook of Biomedical Fluorescence* (Marcel Dekker, New York, 2003)
42. R. Richards-Kortum, E. Sevick-Muraca, Quantitative optical spectroscopy for tissue diagnosis. *Annu. Rev. Phys. Chem.* **47**, 555–606 (1996)
43. N. Ramanujam, Fluorescence spectroscopy of neoplastic and non-neoplastic tissues. *Neoplasia* **2**, 89–117 (2000)
44. K. Sokolov, M. Follen, R. Richards-Kortum, Optical spectroscopy for detection of neoplasia. *Curr. Opin. Chem. Biol.* **6**, 651–658 (2002)
45. T. Vo-Dinh, *Biomedical Photonics Handbook* (CRC Press, Boca Raton, 2003)
46. T. Galeotti, G.D.V. van Rossum, D.H. Mayer, B. Chance, On the fluorescence of NAD(P)H in whole-cell preparation of tumors and normal tissues. *Eur. J. Biochem.* **17**, 485–496 (1970)
47. B. Chance, Optical method. *Annu. Rev. Biophys. Biophys. Chem.* **20**, 1–28 (1991)
48. B. Thorell, B. Chance, Localization and kinetics of reduced pyridine nucleotide in living cells by microfluorometry. *J. Biol. Chem.* **234**, 3044–3050 (1959)
49. Policard, A study on the available aspects of experimental tumours examined by Wood's light. *C. R. Seances Soc. Biol. Fil.* **91**, 1423–1424 (1924)
50. F.N. Ghadially, W.J. Neish, Porphyrin fluorescence of experimentally produced squamous cell carcinoma. *Nature* **188**, 1124 (1960)
51. F.N. Ghadially, Red fluorescence of experimentally induced and human tumours. *J. Pathol. Bacteriol.* **80**, 345 (1960)

52. K.T. Schomacker, J.K. Frisoli, C. Compton, T.J. Flotte, J.M. Richter, N. Nishioka, T.F. Deutsch, Ultraviolet laser-induced fluorescence of colonic tissue: basic biology and diagnostic potential. *Lasers Surg. Med.* **12**, 63–78 (1992)
53. K.D. Ashby, J. Wen, P. Chowdhury, T.A. Casey, M.A. Rasmussen, J.W. Petrich, Fluorescence of dietary porphyrins as a basis for real-time detection of fecal contamination on meat. *J. Agric. Food Chem.* **51**, 3502–3507 (2003)
54. L.F. Ma, D. Dolphin, The metabolites of dietary chlorophylls. *Phytochemistry* **50**, 195–202 (1999)
55. M. Boulton, F. Docchio, P. Dayhaw-Barker, R. Ramponi, R. Cubeddu, Age-related changes in the morphology, absorption and fluorescence of melanosomes and lipofuscin granules of the retinal pigment epithelium. *Vision Res.* **30**, 1291–1303 (1990)
56. C.J. Kennedy, P.E. Rakoczy, I.J. Constable, Lipofuscin of the retinal pigment epithelium: a review. *Eye (Lond.)* **9**(Pt 6), 763–771 (1995)
57. M.B. Ericson, J. Uhre, C. Strandeberg, B. Stenquist, O. Larko, A.M. Wennberg, A. Rosen, Bispectral fluorescence imaging combined with texture analysis and linear discrimination for correlation with histopathologic extent of basal cell carcinoma. *J. Biomed. Opt.* **10**, 034009 (2005)
58. S. Andersson-Engels, G. Canti, R. Cubeddu, C. Eker, C. af Klinteberg, A. Pifferi, K. Svanberg, S. Svanberg, P. Taroni, G. Valentini, I. Wang, Preliminary evaluation of two fluorescence imaging methods for the detection and the delineation of basal cell carcinomas of the skin. *Lasers Surg. Med.* **26**, 76–82 (2000)
59. E. Endlicher, P. Rummele, F. Hausmann, H.C. Rath, R. Knuchel, R.C. Krieg, J. Scholmerich, H. Messmann, Detection of dysplastic lesions by fluorescence in a model of chronic colitis in rats after local application of 5-aminolevulinic acid and its esterified derivatives. *Photochem. Photobiol.* **79**, 189–192 (2004)
60. J. Gahlen, J. Stern, J. Pressmar, J. Bohm, R. Holle, C. Herfarth, Local 5-aminolevulinic acid application for laser light-induced fluorescence diagnosis of early staged colon cancer in rats. *Lasers Surg. Med.* **26**, 302–307 (2000)
61. C. Eker, S. Montan, E. Jaramillo, K. Koizumi, C. Rubio, S. Andersson-Engels, K. Svanberg, S. Svanberg, P. Slezak, Clinical spectral characterisation of colonic mucosal lesions using autofluorescence and delta aminolevulinic acid sensitisation. *Gut* **44**, 511–518 (1999)
62. M. Csanady, J.G. Kiss, L. Ivan, J. Jori, J. Czigner, ALA (5-aminolevulinic acid)-induced protoporphyrin IX fluorescence in the endoscopic diagnosis and control of pharyngolaryngeal cancer. *Eur. Arch. Otorhinolaryngol.* **261**, 262–266 (2004)
63. Y.T. Pan, T.Q. Xie, C.W. Du, S. Bastacky, S. Meyers, M.L. Zeidel, Enhancing early bladder cancer detection with fluorescence-guided endoscopic optical coherence tomography. *Opt. Lett.* **28**, 2485–2487 (2003)
64. M. Olivo, W. Lau, V. Manivasager, T.P. Hoon, C. Christopher, Fluorescence confocal microscopy and image analysis of bladder cancer using 5-aminolevulinic acid. *Int. J. Oncol.* **22**, 523–528 (2003)
65. V. Manivasager, P.W. Heng, J. Hao, W. Zheng, K.C. Soo, M. Olivo, A study of 5-aminolevulinic acid and its methyl ester used in vitro and in vivo systems of human bladder cancer. *Int. J. Oncol.* **22**, 313–318 (2003)
66. R.M. Lycette, R.B. Leslie, Fluorescence of malignant tissue. *Lancet* **2**, 436 (1965)
67. R.R. Alfano, D.B. Tata, J.J. Cordero, P. Tomashefsky, F.W. Longo, M.A. Alfano, Laser induced fluorescence spectroscopy from native cancerous and normal tissue. *IEEE J. Quantum Electron.* **20**, 1507–1511 (1984)
68. W.K. Huh, R.M. Cestero, F.A. Garcia, M.A. Gold, R.S. Guido, K. McIntyre-Seltman, D.M. Harper, L. Burke, S.T. Sum, R.F. Flewelling, R.D. Alvarez, Optical detection of high-grade cervical intraepithelial neoplasia in vivo: results of a 604-patient study. *Am. J. Obstet. Gynecol.* **190**, 1249–1257 (2004)

69. T. DeSantis, N. Chakhtoura, L. Twiggs, D. Ferris, M. Lashgari, L. Flowers, M. Faupel, S. Bambot, S. Raab, E. Wilkinson, Spectroscopic imaging as a triage test for cervical disease: a prospective multicenter clinical trial. *J. Low. Genit. Tract Dis.* **11**, 18–24 (2007)
70. S.K. Chang, M.Y. Dawood, G. Staerkel, U. Utzinger, E.N. Atkinson, R.R. Richards-Kortum, M. Follen, Fluorescence spectroscopy for cervical precancer detection: is there variance across the menstrual cycle? *J. Biomed. Opt.* **7**, 595–602 (2002)
71. I. Georgakoudi, E.E. Sheets, M.G. Muller, V. Backman, C.P. Crum, K. Badizadegan, R.R. Dasari, M.S. Feld, Trimodal spectroscopy for the detection and characterization of cervical precancers in vivo. *Am. J. Obstet. Gynecol.* **186**, 374–382 (2002)
72. N. Ramanujam, M. Follen, A. Mahadevan, S. Thomsen, G. Staerkel, A. Malpica, R. Richards-Kortum, Cervical pre-cancer detection using a multivariate statistical algorithm based on laser induced fluorescence spectra at multiple excitation wavelengths. *Photochem. Photobiol.* **6**, 720–735 (1996)
73. J. Wu, M.S. Feld, R.P. Rava, Analytical model for extracting intrinsic fluorescence in turbid media. *Appl. Opt.* **32**, 3585–3595 (1993)
74. G. Zonios, L. Perelman, V. Backman, R. Manoharan, M. Fitzmaurice, J.V. Dam, M. Feld, Diffuse reflectance spectroscopy of human adenomatous colon polyps in vivo. *Appl. Opt.* **38**, 6628–6637 (1999)
75. L.T. Perelman, V. Backman, M. Wallace, G. Zonios, R. Manoharan, A. Nusrat, S. Shields, M. Seiler, C. Lima, T. Hamano, I. Itzkan, J. Van Dam, J.M. Crawford, M.S. Feld, Observation of periodic fine structure in reflectance from biological tissue: a new technique for measuring nuclear size distribution. *Phys. Rev. Lett.* **80**, 627–630 (1998)
76. S. Lam, T. Kennedy, M. Unger, Y.E. Miller, D. Gelmont, V. Rusch, B. Gipe, D. Howard, J.C. LeRiche, A. Coldman, A.F. Gazdar, Localization of bronchial intraepithelial neoplastic lesions by fluorescence bronchoscopy. *Chest* **113**, 696–702 (1998)
77. P. Pierard, J. Faber, J. Hutsebaut, B. Martin, G. Plat, J.P. Sculier, V. Ninane, Synchronous lesions detected by autofluorescence bronchoscopy in patients with high-grade preinvasive lesions and occult invasive squamous cell carcinoma of the proximal airways. *Lung Cancer* **46**, 341–347 (2004)
78. K. Haussinger, H. Becker, F. Stanzel, A. Kreuzer, B. Schmidt, J. Strausz, S. Cavaliere, F. Herth, M. Kohlhauff, K.M. Muller, R.M. Huber, U. Pichlmeier, T. Bolliger, Autofluorescence bronchoscopy with white light bronchoscopy compared with white light bronchoscopy alone for the detection of precancerous lesions: a European randomised controlled multicentre trial. *Thorax* **60**, 496–503 (2005)
79. H. Hoshino, K. Shibuya, M. Chiyo, A. Iyoda, S. Yoshida, Y. Sekine, T. Iizasa, Y. Saitoh, M. Baba, K. Hiroshima, H. Ohwada, T. Fujisawa, Biological features of bronchial squamous dysplasia followed up by autofluorescence bronchoscopy. *Lung Cancer* **46**, 187–196 (2004)
80. M. Chiyo, K. Shibuya, H. Hoshino, K. Yasufuku, Y. Sekine, T. Iizasa, K. Hiroshima, T. Fujisawa, Effective detection of bronchial preinvasive lesions by a new autofluorescence imaging bronchovideoscope system. *Lung Cancer* **48**, 307–313 (2005)
81. B. Lam, M.P. Wong, S.L. Fung, D.C. Lam, P.C. Wong, T.Y. Mok, F.M. Lam, M.S. Ip, C.G. Ooi, W.K. Lam, The clinical value of autofluorescence bronchoscopy for the diagnosis of lung cancer. *Eur. Respir. J.* **28**, 915–919 (2006)
82. M. Keijzer, R.R. Richards-Kortum, S.L. Jacques, M.S. Feld, Fluorescence spectroscopy of turbid media: autofluorescence of the human aorta. *Appl. Opt.* **28**, 4286–4292 (1989)
83. R. Meerwaldt, R. Graaff, P.H. Oomen, T.P. Links, J.J. Jager, N.L. Alderson, S.R. Thorpe, J.W. Baynes, R.O. Gans, A.J. Smit, Simple non-invasive assessment of advanced glycation endproduct accumulation. *Diabetologia* **47**, 1324–1330 (2004)
84. M. Monami, C. Lamanna, F. Gori, F. Bartalucci, N. Marchionni, E. Mannucci, Skin autofluorescence in type 2 diabetes: beyond blood glucose. *Diabetes Res. Clin. Pract.* **79**, 56–60 (2008)

85. M.J. Noordzij, J.D. Lefrandt, E.A. Loeffen, B.R. Saleem, R. Meerwaldt, H.L. Lutgers, A.J. Smit, C.J. Zeebregts, Skin autofluorescence is increased in patients with carotid artery stenosis and peripheral artery disease. *Int. J. Cardiovasc. Imaging* **28**, 431–438 (2012)
86. R. Meerwaldt, H.L. Lutgers, T.P. Links, R. Graaff, J.W. Baynes, R.O. Gans, A.J. Smit, Skin autofluorescence is a strong predictor of cardiac mortality in diabetes. *Diabetes Care* **30**, 107–112 (2007)
87. R. George, M. Michaelides, M.A. Brewer, U. Utzinger, Parallel factor analysis of ovarian autofluorescence as a cancer diagnostic. *Lasers Surg. Med.* **44**, 282–295 (2012)
88. J.N. McAlpine, S. El Hallani, S.F. Lam, S.E. Kalloger, M. Luk, D.G. Huntsman, C. MacAulay, C.B. Gilks, D.M. Miller, P.M. Lane, Autofluorescence imaging can identify preinvasive or clinically occult lesions in fallopian tube epithelium: a promising step towards screening and early detection. *Gynecol. Oncol.* **120**, 385–392 (2011)
89. T. Matsuda, Y. Saito, K.I. Fu, T. Uraoka, N. Kobayashi, T. Nakajima, H. Ikehara, Y. Mashimo, T. Shimoda, Y. Murakami, A. Parra-Blanco, T. Fujimori, D. Saito, Does autofluorescence imaging videoendoscopy system improve the colonoscopic polyp detection rate?—a pilot study. *Am. J. Gastroenterol.* **103**, 1926–1932 (2008)
90. D. Ramsoekh, J. Haringsma, J.W. Poley, P. van Putten, H. van Dekken, E.W. Steyerberg, M.E. van Leerdam, E.J. Kuipers, A back-to-back comparison of white light video endoscopy with autofluorescence endoscopy for adenoma detection in high-risk subjects. *Gut* **59**, 785–793 (2010)
91. Y. Takeuchi, T. Inoue, N. Hanaoka, K. Higashino, H. Iishi, R. Chatani, M. Hanafusa, T. Kizu, R. Ishihara, M. Tatsuta, T. Shimokawa, N. Uedo, Autofluorescence imaging with a transparent hood for detection of colorectal neoplasms: a prospective, randomized trial. *Gastrointest. Endosc.* **72**, 1006–1013 (2010)
92. K. Moriichi, M. Fujiya, R. Sato, J. Watari, Y. Nomura, T. Nata, N. Ueno, S. Maeda, S. Kashima, K. Itabashi, C. Ishikawa, Y. Inaba, T. Ito, K. Okamoto, H. Tanabe, T. Mizukami, Y. Saitoh, Y. Kohgo, Back-to-back comparison of auto-fluorescence imaging (AFI) versus high resolution white light colonoscopy for adenoma detection. *BMC Gastroenterol.* **12**, 75 (2012)
93. G. Rotondano, M.A. Bianco, S. Sansone, A. Prisco, C. Meucci, M.L. Garofano, L. Cipolletta, Trimodal endoscopic imaging for the detection and differentiation of colorectal adenomas: a prospective single-centre clinical evaluation. *Int. J. Colorectal Dis.* **27**, 331–336 (2012)
94. T. Kuiper, F.J. van den Broek, A.H. Naber, E.J. van Soest, P. Scholten, R. Mallant-Hent, J. van den Brande, J.M. Jansen, A.H. van Oijen, W.A. Marsman, J.J. Bergman, P. Fockens, E. Dekker, Endoscopic trimodal imaging detects colonic neoplasia as well as standard video endoscopy. *Gastroenterology* **140**, 1887–1894 (2011)
95. F.J. van den Broek, P. Fockens, S. Van Eeden, M.A. Kara, J.C. Hardwick, J.B. Reitsma, E. Dekker, Clinical evaluation of endoscopic trimodal imaging for the detection and differentiation of colonic polyps. *Clin. Gastroenterol. Hepatol.* **7**, 288–295 (2009)
96. T.E. Renkoski, B. Banerjee, L.R. Graves, N.S. Rial, S.A. Reid, V.L. Tsikitis, V.N. Nfonam, P. Tiwari, H. Gavini, U. Utzinger, Ratio images and ultraviolet C excitation in autofluorescence imaging of neoplasms of the human colon. *J. Biomed. Opt.* **18**, 16005 (2013)
97. K. Imaizumi, Y. Harada, N. Wakabayashi, Y. Yamaoka, H. Konishi, P. Dai, H. Tanaka, T. Takamatsu, Dual-wavelength excitation of mucosal autofluorescence for precise detection of diminutive colonic adenomas. *Gastrointest. Endosc.* **75**, 110–117 (2012)
98. M.G. Muller, T.A. Valdez, I. Georgakoudi, V. Backman, C. Fuentes, S. Kabani, N. Laver, Z. Wang, C.W. Boone, R.R. Dasari, S.M. Shapshay, M.S. Feld, Spectroscopic detection and evaluation of morphologic and biochemical changes in early human oral carcinoma. *Cancer* **97**, 1681–1692 (2003)
99. V.R. Jacobs, S. Paepke, H. Schaaf, B.C. Weber, M. Kiechle-Bahat, Autofluorescence ductoscopy: a new imaging technique for intraductal breast endoscopy. *Clin. Breast Cancer* **7**, 619–623 (2007)

100. G.M. Palmer, C. Zhu, T.M. Breslin, F. Xu, K.W. Gilchrist, N. Ramanujam, Comparison of multiexcitation fluorescence and diffuse reflectance spectroscopy for the diagnosis of breast cancer. *IEEE Trans. Biomed. Eng.* **50**, 1233–1242 (2003)
101. T.M. Breslin, F. Xu, G.M. Palmer, C. Zhu, K.W. Gilchrist, N. Ramanujam, Autofluorescence and diffuse reflectance properties of malignant and benign breast tissues. *Ann. Surg. Oncol.* **11**, 65–70 (2004)
102. M.A. Kara, J.J. Bergman, Autofluorescence imaging and narrow-band imaging for the detection of early neoplasia in patients with Barrett's esophagus. *Endoscopy* **38**, 627–631 (2006)
103. T.J. Pfefer, D.Y. Paithankar, J.M. Ponerros, K.T. Schomacker, N.S. Nishioka, Temporally and spectrally resolved fluorescence spectroscopy for the detection of high grade dysplasia in Barrett's esophagus. *Lasers Surg. Med.* **32**, 10–16 (2003)
104. I. Georgakoudi, B.C. Jacobson, J. Van Dam, V. Backman, M.B. Wallace, M.G. Müller, Q. Zhang, K. Badizadegan, D. Sun, G.A. Thomas, L.T. Perelman, M.S. Feld, Fluorescence, reflectance, and light-scattering spectroscopy for evaluating dysplasia in patients with Barrett's esophagus. *Gastroenterology* **120**, 1620–1629 (2001)
105. F. Koenig, F.J. McGovern, H. Enquist, R. Lame, T.F. Deutsch, K.T. Schomacker, Autofluorescence guided biopsy for the early diagnosis of bladder carcinoma. *J. Urol.* **159**, 1871–1875 (1998)
106. W. Zheng, W. Lau, C. Cheng, K.C. Soo, M. Olivo, Optimal excitation-emission wavelengths for autofluorescence diagnosis of bladder tumors. *Int. J. Cancer* **104**, 477–481 (2003)
107. D. Frimberger, D. Zaak, H. Stepp, R. Knüchel, R. Baumgartner, P. Schneede, N. Schmeller, A. Hofstetter, Autofluorescence imaging to optimize 5-ALA-induced fluorescence endoscopy of bladder carcinoma. *Urology* **58**, 372–375 (2001)
108. M.C. Jacobson, R. deVere White, S.G. Demos, In vivo testing of a prototype system providing simultaneous white light and near infrared autofluorescence image acquisition for detection of bladder cancer. *J. Biomed. Opt.* **17**, 036011 (2012)
109. Ch. Schäffauer, D. Ettore, M. Rouprêt, V. Phé, J.M. Tualle, E. Tinet, S. Avrillier, Ch. Egrot, O. Traxer, O. Cussenot, Detection of bladder urothelial carcinomas using in vivo non-contact ultraviolet-excited autofluorescence measurements converted into simple colour-coded images: a feasibility study. *Urology* (2013)
110. Y. Sun, N. Hatami, M. Yee, J. Phipps, D.S. Elson, F. Gorin, R.J. Schrot, L. Marcu, Fluorescence lifetime imaging microscopy for brain tumor image-guided surgery. *J. Biomed. Opt.* **15**, 056022 (2010)
111. S.K. Majumder, S. Gebhart, M.D. Johnson, R. Thompson, W.C. Lin, A. Mahadevan-Jansen, A probability-based spectroscopic diagnostic algorithm for simultaneous discrimination of brain tumor and tumor margins from normal brain tissue. *Appl. Spectrosc.* **61**, 548–557 (2007)
112. G.M. van Dam, G. Themelis, L.M. Crane, N.J. Harlaar, R.G. Pleijhuis, W. Kelder, A. Sarantopoulos, J.S. de Jong, H.J. Arts, A.G. van der Zee, J. Bart, P.S. Low, V. Ntziachristos, Intraoperative tumor-specific fluorescence imaging in ovarian cancer by folate receptor-alpha targeting: first in-human results. *Nat. Med.* **17**, 1315–1319 (2011)
113. D.P. Taggart, B. Choudhary, K. Anastasiadis, Y. Abu-Omar, L. Balacumaraswami, D.W. Pigott, Preliminary experience with a novel intraoperative fluorescence imaging technique to evaluate the patency of bypass grafts in total arterial revascularization. *Ann. Thorac. Surg.* **75**, 870–873 (2003)
114. C.P. Parungo, S. Ohnishi, S.W. Kim, S. Kim, R.G. Laurence, E.G. Soltesz, F.Y. Chen, Y.L. Colson, L.H. Cohn, M.G. Bawendi, J.V. Frangioni, Intraoperative identification of esophageal sentinel lymph nodes with near-infrared fluorescence imaging. *J. Thorac. Cardiovasc. Surg.* **129**, 844–850 (2005)
115. S.L. Troyan, V. Kianzad, S.L. Gibbs-Strauss, S. Gioux, A. Matsui, R. Oketokoun, L. Ngo, A. Khamene, F. Azar, J.V. Frangioni, The FLARE intraoperative near-infrared fluorescence imaging system: a first-in-human clinical trial in breast cancer sentinel lymph node mapping. *Ann. Surg. Oncol.* **16**, 2943–2952 (2009)

116. J.C. Rasmussen, I.C. Tan, M.V. Marshall, C.E. Fife, E.M. Sevick-Muraca, Lymphatic imaging in humans with near-infrared fluorescence. *Curr. Opin. Biotechnol.* **20**, 74–82 (2009)
117. C. Regis, P. Collinet, M.O. Farine, S. Mordon, Comparison of aminolevulinic acid- and hexylester aminolevulinic acid-induced protoporphyrin IX fluorescence for the detection of ovarian cancer in a rat model. *Photomed. Laser Surg.* **25**, 304–311 (2007)
118. S. Avrillier, E. Tinet, D. Etori, J.M. Tualle, B. Gelebart, Influence of the emission-reception geometry in laser-induced fluorescence spectra from turbid media. *Appl. Opt.* **37**, 2781–2787 (1998)
119. S. Warren, K. Pope, Y. Yazdi, A.J. Welch, S. Thomsen, A.L. Johnston, M.J. Davis, R. Richards-Kortum, Combined ultrasound and fluorescence spectroscopy for physico-chemical imaging of atherosclerosis. *IEEE Trans. Biomed. Eng.* **42**, 121–132 (1995)
120. J. Qu, C. MacAulay, S. Lam, B. Palcic, Laser-induced fluorescence spectroscopy at endoscopy: tissue optics, Monte Carlo modeling, and in vivo measurements. *Opt. Eng.* **34**, 3334–3343 (1995)
121. J.Y. Qu, J.W. Hua, Calibrated fluorescence imaging of tissue in vivo. *Appl. Phys. Lett.* **78**, 4040–4042 (2001)
122. Q. Zhang, M.G. Muller, J. Wu, M.S. Feld, Turbidity-free fluorescence spectroscopy of biological tissue. *Opt. Lett.* **25**, 1451–1453 (2000)
123. S.K. Chang, D. Arifler, R. Drezek, M. Follen, R. Richards-Kortum, Analytical model to describe fluorescence spectra of normal and preneoplastic epithelial tissue: comparison with Monte Carlo simulations and clinical measurements. *J. Biomed. Opt.* **9**, 511–522 (2004)
124. S. Yuan, C.A. Roney, J. Wierwille, C. Chen, B. Xu, J. Jiang, H. Ma, A. Cable, R.M. Summers, Y. Chen, Combining optical coherence tomography with fluorescence molecular imaging: towards simultaneous morphology and molecular imaging. *Phys. Med. Biol.* **55**, 191–206 (2010)
125. R.V. Kuranov, V.V. Sapozhnikova, H.M. Shakhova, V.M. Gelikonov, E.V. Zagainova, S.A. Petrova, Combined application of optical methods to increase the information content of optical coherent tomography in diagnostics of neoplastic processes. *Quantum Electron.* **32**, 993–998 (2002)
126. U. Utzinger, R.R. Richards-Kortum, Fiber optic probes for biomedical optical spectroscopy. *J. Biomed. Opt.* **8**, 121–147 (2003)
127. S.J. Oldenburg, R.D. Averitt, S.L. Westcott, N.J. Halas, Nanoengineering of optical resonances. *Chem. Phys. Lett.* **288**, 243–247 (1998)
128. G.M. Dobre, A.G. Podoleanu, R.B. Rosen, Simultaneous optical coherence tomography – indocyanine green dye fluorescence imaging system for investigations of the eye’s fundus. *Opt. Lett.* **30**(1), 58–60 (2005)
129. E. Beaupaire, L. Moreaux, F. Amblard, J. Mertz, Combined scanning optical coherence and two-photon-excited fluorescence spectroscopy. *Opt. Lett.* **24**, 969–971 (1999)
130. S. Glass, TIE-36 fluorescence of optical glass, in *Technical Information, Optics for Devices*. (2004)
131. K.R. Hawkins, P. Yager, Nonlinear decrease of background fluorescence in polymer thin-films – a survey of materials and how they can complicate fluorescence detection in microTAS. *Lab Chip* **3**(4), 248–252 (2003)
132. M.J. Hodgkin, Epoxies for optoelectronic packaging; applications and material properties. *J. Microelectron. Electron. Packag.* **1**(2), 108–116 (2004)
133. J. Wu, S. Seregard, P.V. Alverer, Photochemical damage of the retina. *Surv. Ophthalmol.* **51**, 461–481 (2006)
134. American National Standards Institute, *American National Standard for Safe Use of Lasers* (ANSI, New York, 2000)
135. American Conference of Governmental Industrial Hygienists, *2005 TLVs and BEIs* (ACGIH, Cincinnati, 2005)

136. International Commission on Non-Ionizing Radiation Protection, Guidelines on limits of exposure to laser radiation of wavelengths between 180 nm and 1,000 microm. *Health Phys.* **71**, 804–819 (1996)
137. International Commission on Non-ionizing Radiation Protection, Revision of guidelines on limits of exposure to laser radiation of wavelengths between 400 nm and 1.4 microm. *Health Phys.* **79**, 431–440 (2000)
138. International Commission on Non-Ionizing Radiation Protection, Guidelines on limits of exposure to ultraviolet radiation of wavelengths between 180 nm and 400 nm (incoherent optical radiation). *Health Phys.* **87**, 171–186 (2004)
139. International Commission on Non-Ionizing Radiation and Protection, Guidelines on limits of exposure to broad-band incoherent optical radiation (0.38 to 3 microm). *Health Phys.* **73**, 539–554 (1997)
140. Center for Devices and Radiological Health, *Guidance for Industry: Electro-Optical Sensors for the In Vivo Detection of Cervical Cancer and Its Precursors: Submission Guidance for an IDE/PMA* (US Department of Health and Human Services, New York, 1998)
141. A.F. Fercher, W. Drexler, C.K. Hitzenberger, Optical coherence tomography-principles and applications. *Rep. Prog. Phys.* **66**, 239–303 (2003)
142. C.F. Zhu, Q. Liu, N. Ramanujam, Effect of fiber optic probe geometry on depth-resolved fluorescence measurements from epithelial tissues: a Monte Carlo simulation. *J. Biomed. Opt.* **8**, 237–247 (2003)
143. Z. Changfang, L. Quan, N. Ramanujam, Effect of fiber optic probe geometry on depth-resolved fluorescence measurements from epithelial tissues: a Monte Carlo simulation. *J. Biomed. Opt.* **8**, 237–247 (2003)
144. T.J. Pfefer, K.T. Schomacker, M.N. Ediger, N.S. Nishioka, Multiple-fiber probe design for fluorescence spectroscopy in tissue. *Appl. Opt.* **41**, 4712–4721 (2002)
145. T.J. Pfefer, L.S. Matchette, A.M. Ross, M.N. Ediger, Selective detection of fluorophore layers in turbid media: the role of fiber-optic probe design. *Opt. Lett.* **28**, 120–122 (2003)
146. T.J. Pfefer, L.S. Matchette, R. Drezek, Influence of illumination-collection geometry on fluorescence spectroscopy in multilayer tissue. *Med. Biol. Eng. Comput.* **42**, 669–673 (2004)
147. J. Wang, P.T. Bender, U. Utzinger, R. Drezek, Depth sensitive reflectance measurements using oblique oriented fiber probes. *J. Biomed. Opt.* **20**, 44017 (2006)
148. M.C. Skala, G.M. Palmer, C.F. Zhu, Q. Liu, K.M. Vrotsos, C.L. Marshak-Stone, A. Gendron-Fitzpatrick, N. Ramanujam, Investigation of fiber-optic probe designs for optical spectroscopic diagnosis of epithelial pre-cancers. *Lasers Surg. Med.* **34**, 25–38 (2004)
149. Q. Liu, N. Ramanujam, Experimental proof of the feasibility of using an angled fiber-optic probe for depth-sensitive fluorescence spectroscopy of turbid media. *Opt. Lett.* **29**, 2034–2036 (2004)
150. T. Papaioannou, N.W. Preyer, Q.Y. Fang, A. Brightwell, M. Carnohan, G. Cottone, R. Ross, L.R. Jones, L. Marcu, Effects of fiber-optic probe design and probe-to-target distance on diffuse reflectance measurements of turbid media: an experimental and computational study at 337 nm. *Appl. Opt.* **43**, 2846–2860 (2004)
151. R.A. Schwarz, D. Arifler, S.K. Chang, I. Pavlova, I.A. Hussain, V. Mack, B. Knight, R. Richards-Kortum, A.M. Gillenwater, Ball lens coupled fiber-optic probe for depth-resolved spectroscopy of epithelial tissue. *Opt. Lett.* **30**, 1159–1161 (2005)
152. A.M.J. Wang, J.E. Bender, J. Pfefer, U. Utzinger, R.A. Drezek, Depth-sensitive reflectance measurements using obliquely oriented fiber probes. *J. Biomed. Opt.* **10**, 44017 (2005)
153. B.W. Pogue, G. Burke, Fiber-optic bundle design for quantitative fluorescence measurement from tissue. *Appl. Opt.* **37**, 7429–7436 (1998)
154. P.R. Bargo, S.A. Prah, S.L. Jacques, Optical properties effects upon the collection efficiency of optical fibers in different probe configurations. *IEEE J. Sel. Top. Quantum Electron.* **9**, 314–321 (2003)

155. S.Y. Ryu, H.Y. Choi, J. Na, E.S. Choi, B.H. Lee, Combined system of optical coherence tomography and fluorescence spectroscopy based on double-cladding fiber. *Opt. Lett.* **33**, 2347–2349 (2008)
156. G. Liu, Z. Chen, Fiber-based combined optical coherence and multiphoton endomicroscopy. *J. Biomed. Opt.* **16**, 036010 (2011)
157. J. Xi, Y. Chen, Y. Zhang, K. Murari, M. Li, X. Li, Integrated multimodal endomicroscopy platform for simultaneous en face optical coherence and two-photon fluorescence imaging. *Opt. Lett.* **37**, 362–364 (2012)
158. J. Mavadia, J. Xi, Y. Chen, X. Li, An all-fiber-optic endoscopy platform for simultaneous OCT and fluorescence imaging. *Biomed. Opt. Express* **3**(11), 2851–2859 (2012)
159. H. Makhlof, A.R. Rouse, A.F. Gmitro, Dual modality fluorescence confocal and spectral-domain optical coherence tomography microendoscope. *Biomed. Opt. Express* **2**(3), 634–644 (2011)
160. S. Schmitz-Valckenberg, F.G. Holz, A.C. Bird, R.F. Spaide, Fundus autofluorescence imaging: review and perspectives. *Retina* **28**(3), 385–409 (2008)
161. H.M. Helb, P. Charbel Issa, M. Fleckenstein, S. Schmitz-Valckenberg, H.P. Scholl, C.H. Meyer, N. Eter, F.G. Holz, Clinical evaluation of simultaneous confocal scanning laser ophthalmoscopy imaging combined with high-resolution, spectral-domain optical coherence tomography. *Acta Ophthalmol.* **88**(8), 842–849 (2010)
162. R.B. Rosen, M. Hathaway, J. Rogers, J. Pedro, P. Garcia, G.M. Dobre, A.G. Podoleanu, Simultaneous OCT/SLO/ICG imaging. *Invest. Ophthalmol. Vis. Sci.* **50**(2), 851–860 (2009)
163. J. Mavadia, X.J. Xi, Y. Chen, X. Li, An all-fiber-optic endoscopy platform for simultaneous OCT and fluorescence imaging. *Biomed. Opt. Express* **3**, 2851–2859 (2012)
164. R. Andrew Wall, J.K. Barton, Fluorescence-based surface magnifying chromoendoscopy and optical coherence tomography endoscope. *J. Biomed. Opt.* **17**(8), 086003 (2012)
165. C.J. Kennedy, P.E. Rakoczy, I.J. Constable, Lipofuscin of the retinal pigment epithelium: a review. *Eye* **9**(6), 763–771 (1995)
166. M. Fleckenstein, S. Schmitz-Valckenberg, C. Adrion, I. Krämer, N. Eter, H.M. Helb, C.K. Brinkmann, P. Charbel Issa, U. Mansmann, F.G. Holz, Tracking progression with spectral-domain optical coherence tomography in geographic atrophy caused by age-related macular degeneration. *Invest. Ophthalmol. Vis. Sci.* **51**(8), 3846–3852 (2010)
167. E.M. Kanter, R.M. Walker, S.L. Marion, M. Brewer, P.B. Hoyer, J.K. Barton, Dual modality imaging of a novel rat model of ovarian carcinogenesis. *J. Biomed. Opt.* **11**, 041123 (2006)
168. A.R. Tumlinson, L.P. Hariri, U. Utzinger, J.K. Barton, A miniature endoscope for simultaneous OCT-LIF measurement. *Appl. Opt.* **43**, 113–121 (2004)
169. L.P. Hariri, E.R. Liebmann, S.L. Marion, P.B. Hoyer, J.R. Davis, M.A. Brewer, J.K. Barton, Simultaneous optical coherence tomography and laser induced fluorescence imaging in rat model of ovarian carcinogenesis. *Cancer Biol. Ther.* **10**(5), 1–10 (2010)
170. L.P. Hariri, A.R. Tumlinson, N.H. Wade, D. Besselsen, U. Utzinger, E. Gerner, J.K. Barton, Endoscopic optical coherence tomography and laser induced fluorescence spectroscopy in a murine colon cancer model. *Lasers Surg. Med.* **38**, 305–313 (2006)
171. J. McNally, N. Kirkpatrick, L.P. Hariri, A.R. Tumlinson, D. Besselsen, E. Gerner, U. Utzinger, J.K. Barton, Task based imaging of colon cancer in a mouse model (*Apc^{Min/+}*). *Appl. Opt.* **45**, 3049–3062 (2006)
172. A.M. Winkler, P. Rice, J. Weichsel, J. Watson, M. Backer, J. Backer, J.K. Barton, In vivo, dual modality OCT/LIF imaging using a novel VEGF receptor targeted NIR fluorescent probe in the AOM-treated mouse model. *Mol. Imaging Biol.* **13**(6), 1173–1182 (2011)
173. J.A. Freeberg, J.L. Benedet, C. MacAulay, L.A. West, M. Follen, The performance of fluorescence and reflectance spectroscopy for the in vivo diagnosis of cervical neoplasia; point probe versus multispectral approaches. *Gynecol. Oncol.* **107**, S248–S255 (2007)

174. R.D. Alvarez, T.C. Wright, Effective cervical neoplasia detection with a novel optical detection system: a randomized trial. *Gynecol. Oncol.* **104**, 281–289 (2007)
175. N. Ramanujam, M.F. Mitchell, A. Mahadevan, S. Thomsen, A. Malpica, T. Wright, N. Atkinson, R. Richards-Kortum, Development of a multivariate statistical algorithm to analyze human cervical tissue fluorescence spectra acquired in vivo. *Lasers Surg. Med.* **19**, 46–62 (1996)
176. T.E. Renkoski, K.D. Hatch, U. Utzinger, Wide-field spectral imaging of human ovary autofluorescence and oncologic diagnosis via previously collected probe data. *J. Biomed. Opt.* **17**, 036003 (2012)
177. S.D. Kamath, R.A. Bhat, S. Ray, K.K. Mahato, Autofluorescence of normal, benign, and malignant ovarian tissues: a pilot study. *Photomed. Laser Surg.* **27**, 325–335 (2009)
178. T. Upile, W.K. Jerjes, H.J. Sterenborg, B.J. Wong, A.K. El-Naggar, J.F. Ilgner, A. Sandison, M.J. Witjes, M.A. Biel, R. van Veen, Z. Hamdoon, A. Gillenwater, C.A. Mosse, D.J. Robinson, C.S. Betz, H. Stepp, L. Bolotine, G. McKenzie, H. Barr, Z. Chen, K. Berg, A.K. D’Cruz, H. Sudhoff, N. Stone, C. Kendall, S. Fisher, A.J. MacRobert, A. Leunig, M. Olivo, R. Richards-Kortum, K.C. Soo, V. Bagnato, L.P. Choo-Smith, K. Svanberg, I.B. Tan, B.C. Wilson, H. Wolfsen, I. Bigio, A.G. Yodh, C. Hopper, At the frontiers of surgery: review. *Head Neck Oncol.* **3**(1), 7 (2011)
179. A.F. Zuluaga, N. Vigneswaran, R.K. Bradley, A.M. Gillenwater, C.M. Nichols, C. Poh, Identafi[®]3000 ultra a multispectral tool for improved oral lesion evaluation, in *Biomedical Optics, OSA Technical Digest (CD)* (Optical Society of America, paper BSuD105, 2010)
180. P.M. Lane, T. Gilhuly, P. Whitehead, H. Zeng, C.F. Poh, S. Ng, P.M. Williams, L. Zhang, M.P. Rosin, C.E. MacAulay, Simple device for the direct visualization of oral-cavity tissue fluorescence. *J. Biomed. Opt.* **11**, 024006 (2006)
181. E. Svistun, R. Alizadeh-Naderi, A. El-Naggar, R. Jacob, A. Gillenwater, R. Richards-Kortum, Vision enhancement system for detection of oral cavity neoplasia based on autofluorescence. *Head Neck* **26**, 205–215 (2004)
182. U. Utzinger, M. Bueeler, S. Oh, D.L. Heintzelman, E.S. Svistun, M. Abd-El-Barr, A. Gillenwater, R. Richards-Kortum, Optimal visual perception and detection of oral cavity neoplasia. *IEEE Trans. Biomed. Eng.* **50**, 396–399 (2003)
183. D.L. Heintzelman, U. Utzinger, H. Fuchs, A. Zuluaga, K. Gossage, A.M. Gillenwater, R. Jacob, B. Kemp, R.R. Richards-Kortum, Optimal excitation wavelengths for in vivo detection of oral neoplasia using fluorescence spectroscopy. *Photochem. Photobiol.* **72**, 103–113 (2000)
184. C.S. Betz, H. Stepp, P. Janda, S. Arbogast, G. Grevers, R. Baumgartner, A. Leunig, A comparative study of normal inspection, autofluorescence and 5-ALA-induced PPIX fluorescence for oral cancer diagnosis. *Int. J. Cancer* **97**(2), 245–252 (2002)
185. A. Gillenwater, R. Jacob, R. Ganeshappa, B. Kemp, A.K. El-Naggar, J.L. Palmer, G. Clayman, M.F. Mitchell, R. Richards-Kortum, Noninvasive diagnosis of oral neoplasia based on fluorescence spectroscopy and native tissue autofluorescence. *Arch. Otolaryngol. Head Neck Surg.* **124**, 1251–1258 (1998)
186. M.V. Chowdary, K.K. Mahato, K.K. Kumar, S. Mathew, L. Rao, C.M. Krishna, J. Kurien, Autofluorescence of breast tissues: evaluation of discriminating algorithms for diagnosis of normal, benign, and malignant conditions. *Photomed. Laser Surg.* **27**, 241–252 (2009)
187. Z. Volynskaya, A.S. Haka, K.L. Bechtel, M. Fitzmaurice, R. Shenk, N. Wang, J. Nazemi, R.R. Dasari, M.S. Feld, Diagnosing breast cancer using diffuse reflectance spectroscopy and intrinsic fluorescence spectroscopy. *J. Biomed. Opt.* **13**(2), 024012 (2008)
188. C. Zhu, G.M. Palmer, T.M. Breslin, F. Xu, N. Ramanujam, Use of a multiseperation fiber optic probe for the optical diagnosis of breast cancer. *J. Biomed. Opt.* **10**, 024032 (2005)
189. P.K. Gupta, S.K. Majumder, A. Uppal, Breast cancer diagnosis using N2 laser excited autofluorescence spectroscopy. *Lasers Surg. Med.* **21**(5), 417–422 (1997)

190. J. Haringsma, G.N. Tytgat, H. Yano, H. Iishi, M. Tatsuta, T. Ogihara, H. Watanabe, N. Sato, N. Marcon, B.C. Wilson, R.W. Cline, Autofluorescence endoscopy: feasibility of detection of GI neoplasms unapparent to white light endoscopy with an evolving technology. *Gastrointest. Endosc.* **53**, 642–650 (2001)
191. N. Uedo, K. Higashino, R. Ishihara, Y. Takeuchi, H. Iishi, Diagnosis of colonic adenomas by new autofluorescence imaging system: a pilot study. *Digest. Endosc.* **19**, S134–S138 (2007)
192. K.T. Schomacker, J.K. Frisoli, C.C. Compton, T.J. Flotte, J.M. Richter, N.S. Nishioka, T.F. Deutsch, Ultraviolet laser-induced fluorescence of colonic tissue: basic biology and diagnostic potential. *Lasers Surg. Med.* **12**, 63–78 (1992)
193. M.A. Ortner, B. Ebert, E. Hein, K. Zumbusch, D. Nolte, U. Sukowski, J. Weber-Eibel, B. Fleige, M. Dietel, M. Stolte, G. Oberhuber, R. Porschen, B. Klump, H. Hortnagl, H. Lochs, H. Rinneberg, Time gated fluorescence spectroscopy in Barrett's oesophagus. *Gut* **52**, 28–33 (2003)
194. W.C. Lin, S.A. Toms, M. Johnson, E.D. Jansen, A. Mahadevan-Jansen, In vivo brain tumor demarcation using optical spectroscopy. *Photochem. Photobiol.* **73**, 396–402 (2001)
195. A. Sivaramakrishnan, D. Graupe, Brain tumor demarcation by applying a LAMSTAR neural network to spectroscopy data. *Neurol. Res.* **26**, 613–621 (2004)
196. W. Drexler, U. Morgner, F.X. Kartner, C. Pitris, S.A. Boppart, X.D. Li, E.P. Ippen, J.G. Fujimoto, In vivo ultrahigh-resolution optical coherence tomography. *Opt. Lett.* **24**, 1221–1223 (1999)
197. B.E. Bouma, G.J. Tearney, I.P. Bilinsky, B. Golubovic, J.G. Fujimoto, Self-phase-modulated Kerr-lens mode-locked Cr:forsterite laser source for optical coherence tomography. *Opt. Lett.* **21**, 1839–1841 (1996)
198. I. Hartl, X.D. Li, C. Chudoba, R.K. Ghanta, T.H. Ko, J.G. Fujimoto, J.K. Ranka, R.S. Windeler, Ultrahigh-resolution optical coherence tomography using continuum generation in an air-silica microstructure optical fiber. *Opt. Lett.* **26**, 608–610 (2001)
199. N.D. Kirkpatrick, J.B. Hoying, S.K. Botting, J.A. Weiss, U. Utzinger, In vitro model for endogenous optical signatures of collagen. *J. Biomed. Opt.* **11**, 054021 (2006)
200. N.D. Kirkpatrick, C.P. Zou, M.A. Brewer, W.R. Brands, R.A. Drezek, U. Utzinger, Endogenous fluorescence spectroscopy of cell suspensions for chemopreventive drug monitoring. *Photochem. Photobiol.* **81**, 125–134 (2005)
201. J.M. Dixon, M. Taniguchi, J.S. Lindsey, PhotochemCAD 2: a refined program with accompanying spectral databases for photochemical calculations. *Photochem. Photobiol.* **81**, 212–213 (2005)
202. M. Bruchez, M. Moronne, P. Gin, S. Weiss, A.P. Alivisatos, Semiconductor nanocrystals as fluorescent biological labels. *Science* **281**, 2013–2016 (1998)
203. A.M. Smith, S. Nie, Chemical analysis and cellular imaging with quantum dots. *Analyst* **129**, 672–677 (2004)
204. R.C. Benson, H.A. Kues, Fluorescence properties of indocyanine green as related to angiography. *Phys. Med. Biol.* **23**, 159–163 (1978)
205. B.R. Hyun, H. Chen, D.A. Rey, F.W. Wise, C.A. Batt, Near-infrared fluorescence imaging with water-soluble lead salt quantum dots. *J. Phys. Chem. B* **111**, 5726–5730 (2007)